

On the Potential of Microtubules for Scalable Quantum Computation

Nick E. Mavromatos^{1,2}, Andreas Mershin^{3,4,8}, and Dimitri V. Nanopoulos^{5,6,7}

¹ *Physics Division, School of Applied Mathematical and Physical Sciences,*

National Technical University of Athens, Zografou Campus, Athens 157 80, Greece

² *Theoretical Particle Physics and Cosmology Group,*

Department of Physics, King's College London, London, WC2R 2LS, UK

³ *MIT Sloan School of Management, 77 Massachusetts Ave. Massachusetts Institute of Technology, Cambridge, MA 02139, USA*

⁴ *RealNose.ai, 626 Massachusetts Ave., 2nd Floor, Arlington, MA 02476, USA*

⁵ *Academy of Athens, Division of Natural Sciences, Athens 10679, Greece*

⁶ *George P. and Cynthia W. Mitchell Institute for Fundamental Physics and Astronomy, Texas A & M University, College Station, TX 77843, USA*

⁷ *Theoretical Physics Department, CERN, CH-1211 Geneva 23, Switzerland and*

⁸ *The OsmoCosm Public Benefit Foundation, www.OsmoCosm.org Boston, MA, USA*

We examine the quantum coherence properties of tubulin heterodimers in the Microtubule (MT) lattice. In the cavity-MT model proposed by the authors, according to which the MT interiors are modeled as high-Q quantum-electrodynamics cavities, decoherence-resistant entangled states have been argued to emerge under physiological conditions, with decoherence times of order $\mathcal{O}(10^{-6})$ s. The latter is the result of strong electric-dipole interactions of tubulin dimers with ordered-water dipole quanta in the MT interior. We re-interpret the classical nonlinear (pseudospin) σ -models, describing the emergent dynamics of solitonic excitations in such systems, as representing quantum coherent (or possibly pointer) states, arising from the incomplete collapse of quantum-coherent dipole states. These solitons mediate dissipation-free energy transfer across the MT networks. We underpin logic-gate-like behavior through MT-associated proteins and detail how these structures may support scalable, ambient-temperature quantum computation, with the fundamental unit of information storage being a quDit associated with the basic unit of the MT honeycomb lattice. We describe in detail the decision-making process, after the action of an external stimulus, during which optimal path selection for energy-loss-free signal and information transport across the MT network emerges. Finally, we propose experimental pathways, including Rabi-splitting spectroscopy and entangled surface plasmon probes, to experimentally validate our predictions for MT-based, scalable quantum computation.

I. INTRODUCTION: SOLITONS, DISSIPATIONLESS ENERGY TRANSFER AND QUANTUM ENTANGLEMENT IN BIOSYSTEMS

One open issue, relevant to using biomatter for quantum computation, as discussed in [1] in the context of a model for biological microtubules (MT) [2] represented as high-quality quantum-electrodynamics (QED) cavities [3, 4], is the efficiency by which energy (and therefore information) is transduced and transported in biosystems. Specifically, in our works we have argued how the QED cavity model of MT can be essential, and in fact unavoidable, for brain functioning [5], in the sense of transforming the trapped information from sources (stimuli) outside the brain into appropriate electromagnetic signals, which are sent and received by the neurons, resulting in exclusively electromagnetic communication through, *e.g.* synapses. QED Cavities are known for providing a very efficient way of manipulating quantum entanglement of atoms and photons [6]. In a similar way, we have proposed in [3] that electric dipole quanta of the tubulin dimer walls of the cavity interiors of the MT, are entangled with the dipole quanta in the ordered-water interior, leading to solitonic structures of such dipoles, which can transfer energy and signal in a dissipation-free way. By representing these MT dipole systems in terms of condensed-matter models, *e.g.* pseudospin non-linear σ -models as in [7], one can quantify such processes of loss-free energy and signal transduction by means of concrete solitonic solutions of the equations of motion of these models. In our picture, as we discuss in [1, 3, 4] and in this article, such classical solitons may be viewed as a kind of coherent states of the dipole quanta.¹

Classical physics allows dissipation-free transport of energy by means of solitons [10], that are well-established classical field theory configurations. The role of biological solitons in efficient energy and signal transmission, has a long, distinguished history going back to seminal publications by H. Fröhlich [11] and A.S. Davydov [12]. The former showed that observable effects of quantum coherent phenomena in biological systems can occur through coherent excitations in the microwave region due to nonlinear couplings between biomolecular dipoles, leading to solitonic

¹ Given that MT are ubiquitous structures in all eukaryotic cells [2], we expect such properties to characterize all living biological matter. For instance, recently it has been made possible to transplant RNA molecules, which are known to carry memory and encode information [8], between snails, by literally injecting one snail's memories into another snail [9], that is passing down RNA through flesh instead of an intact nervous system. Since living cells produce or modify RNA through the action of external stimuli, our model for information processing may therefore apply to such biological structures as well.

configurations responsible for loss-free energy (i.e. dissipationless) signaling. The ‘pumping’ frequency of such coherent modes was established to be of order of the inverse of Fröhlich’s coherence time $t_{\text{coherence Fröhlich}} \sim 10^{-11} - 10^{-12}$ s.

Davydov[12], subsequently proposed the existence of *solitonic excitation states* along the α -helix self-trapped amide treatment bearing a striking mathematical similarity to superconductivity. The α -helix lattice is characterised by two kinds of excitations: deformational oscillations, which result in quantized excitations similar to “phonons” in the case of superconductivity, and internal amide excitations. The non-linear coupling between these two types of excitations gives rise to a soliton, which traps the vibrational energy of the α -helix, thereby preventing its distortion, and thus resulting in dissipation-free energy transport.

It should be stressed that, although the solitons appear as classical solutions of certain field equations, nonetheless their appearance is the explicit result of quantum coherent states. However, due to the extremely complex environment of biological entities, one expects the quantum effects to decohere [13] quite quickly, thus making the conditions for the appearance of coherent states, that could lead to solitons, very delicate, but not impossible, to be realised in nature.²

In the 1990’s, a suggestion on the rôle of quantum effects on brain functioning, and in particular on conscious perception, has been put forward by S. Hameroff and R. Penrose (HP) [15], who concentrated on the microtubules (MT) [2] of the brain cells. Specifically, by considering the tubulin heterodimers conformation as quantum states of a two-state system, they assumed their coherent superposition, which may result in helicoidal solitonic states propagating along the MT,³ and thus being responsible for conscious perception. HP assumed sufficiently long decoherence time for this purpose of order $\mathcal{O}(1 \text{ s})$ in *in vivo* situations, so that the *in vivo* system of MT in the brain undergoes, as a result of sufficient growth that allowed it to reach a critical mass/energy, *self-collapse* related to a *quantum gravity* environment (orchestrated reduction method), as opposed to the standard *environmental non-gravitational decoherence* that physical quantum systems are subjected to [13].

In our discussion below we shall not adopt the approach of HP [15] on understanding consciousness, but we shall be dealing with more mundane questions, as to whether appropriate solitonic states in MT stem from quantum effects, thus behaving as coherent (or even pointer [16] states, which had not completely decohered) and whether there are units inside a MT network that play a crucial rôle in ‘decision’ making regarding the optimal path for information and energy transduction.

To make the above ideas on the potentially important role of solitons in biological systems clearer to the reader, we first briefly review the relevant basic properties of solitons [10], in the framework of a toy field-theoretic model. Solitons are *finite energy* classical solutions of the Lagrange equations stemming from appropriate field theories. Given the properties of solitons salient to dissipationless energy and signal transduction, it is sufficient (but also directly relevant to the case of biological systems such as microtubular networks), to consider a flat-spacetime (1+1)-dimensional field theory of an interacting scalar field $\phi(t, x)$ with potential $V(\phi)$ and action (for our discussion of soliton solutions below, we use units $\hbar = c = 1$, for convenience):

$$\mathcal{S} = \int dt dx \left(\frac{1}{2} (\partial_t \phi)^2 - \frac{1}{2} (\partial_x \phi)^2 - V(\phi) \right). \quad (1)$$

We consider potentials with two non-trivial minima, at $\phi = \pm C$, as in fig. 1. A typical form is given by:

$$V(\Phi) = V_0 (C^2 - \phi^2)^2, \\ \text{where e.g. } V_0 = \frac{\lambda}{4}, \quad C^2 = \frac{m^2}{\lambda}, \quad m > 0, \lambda > 0. \quad (2)$$

The total energy functional is given by the spatial integral:

$$E = \int dx \left(\frac{1}{2} (\partial_t \phi)^2 + \frac{1}{2} (\partial_x \phi)^2 + V(\phi) \right). \quad (3)$$

The Euler-Lagrange equations of motion (EoM) stemming from (1) read:

$$\partial_t^2 \phi - \partial_x^2 \phi = -\frac{\delta V}{\delta \phi}. \quad (4)$$

² It should be mentioned, at this point, that the question whether quantum effects play a rôle in biophysical systems is much older than the abovementioned works, and dates back to Schrödinger [14], who argued that certain aspects of life, such as mutations in living organisms (that is, changes in the DNA sequence of a cell’s genom or a virus), might not be explainable by classical physics but require quantum concepts, such as quantum leaps.

³ Note that the helix is a geodesic path (optimal “minimum distance” path) in the Euclidean cylindrical geometry $S^1 \otimes \mathbb{R}$, embeddable in \mathbb{R}^3 .

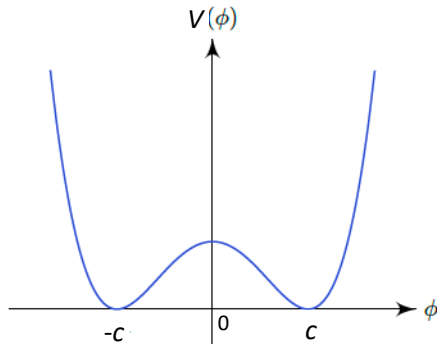


FIG. 1. A typical potential, with two degenerate non-trivial minima at $\phi = \pm C$, for a soliton solution in a (1+1)-dimensional real-scalar ϕ field theory.

Solitons are solutions of (4), for which the energy functional (3) is *finite*. The important feature of solitons is that they are localised solutions, which retain their shape upon propagating freely, but also under collisions among themselves. It is such properties that play a crucial rôle in treating solitons as the enablers of loss-free energy transfer, but also as bio- “logic gates”, as we shall discuss below.

To construct a soliton, we first find a static solution to (4), *i.e.* $\partial_t \phi = 0$, and then perform a Lorentz boost, with velocity v along the x -direction. The boost is characterized by $\partial_t^2 \phi = 0$. Multiplying the static EoM (4) by $\partial_x \phi \equiv \phi'$, we obtain the non-linear equation $0 = \phi'' \phi' - \frac{\delta V}{\delta \phi} \phi' = \frac{d}{dx} \left(\frac{1}{2} (\phi')^2 - V(\phi) \right)$, which can be straightforwardly integrated over x , yielding (upon setting the appropriate constants to zero):

$$\begin{aligned} \frac{1}{2} (\phi')^2 = V(\phi) &\Rightarrow \phi' = \pm \sqrt{2V(\phi)} \\ x - x_0 = \pm \int_{\phi(x_0)}^{\phi(x)} \frac{d\tilde{\phi}}{\sqrt{2V(\tilde{\phi})}}. \end{aligned} \quad (5)$$

The \pm signature in the right hand side of the middle and final equations is the origin of the *chiral* unintuitive nature of the soliton.

For specific families of the potential (2), the corresponding soliton solutions are determined by the requirement that the field solutions asymptote (as $x \rightarrow \pm\infty$) to the vacuum values:

$$\lim_{x \rightarrow \pm\infty} \phi(x) = \pm\sqrt{C} = \pm \frac{m}{\sqrt{\lambda}}. \quad (6)$$

For the ϕ^4 potential (2), the inversion of the expression (5) yields the celebrated static (anti) kink soliton solution [10]:

$$\phi(x) = \pm \frac{m}{\sqrt{\lambda}} \tanh\left(\frac{m}{\sqrt{2}}(x - x_0)\right), \quad (7)$$

which satisfies the boundary conditions (6) (*cf.* fig. 2).

The energy density $\mathcal{E}(x)$ of the kink is determined from the integrand of (3), as:

$$\mathcal{E}(x) = \frac{m^4}{2\lambda} \operatorname{sech}^4\left(\frac{m}{\sqrt{2}}(x - x_0)\right), \quad (8)$$

and, therefore, its total mass (total rest energy) is given by:

$$M = \int_{-\infty}^{\infty} \mathcal{E}(x) dx = \frac{2\sqrt{2}}{3} \frac{m^3}{\lambda}, \quad (9)$$

and it is conserved in time, that is one gets the same value upon using the boosted kink solution (traveling wave), obtained from (7) by the replacement $x - x_0 \rightarrow \gamma(x - x_0 - vt)$, $\gamma = (1 - v^2)^{-1/2}$, as already mentioned:

$$\phi(t, x) = \pm \frac{m}{\sqrt{\lambda}} \tanh\left(\frac{m}{\sqrt{2}} \gamma(x - x_0 - vt)\right). \quad (10)$$

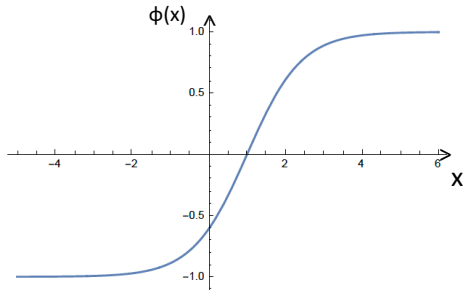


FIG. 2. The profile of a typical one-dimensional static kink soliton (7) (pictured here for indicative values $m = \sqrt{\lambda} = 1$, and $x_0 = 1$). The same profile characterizes the traveling kink wave (10), obtained upon the replacement of $x - x_0$ in (7) by the Lorentz boosted coordinate $\gamma(x - x_0 - vt)$, $\gamma = \frac{1}{\sqrt{1-v^2}}$, where $v > 0 (< 0)$ corresponds to left (right) movers.

The way the solitons behave at spatial infinity ($x = \pm\infty$) imply that it takes an infinite amount of energy to change the (anti)kink configuration. This is an indication of its stability, but the latter is also a guarantee -rigorously for topological reasons. Indeed, for the system (1), although there are no Noether currents associated with a symmetry of the real scalar field, nevertheless, there is a (trivially) conserved current

$$\mathcal{J}^\mu = \frac{1}{2} \frac{\sqrt{\lambda}}{m} \epsilon^{\mu\nu} \partial_\nu \phi, \quad (11)$$

where $\epsilon^{\mu\nu}$ is the Levi-Civita symbol in the (1+1)-dimensional Minkowski spacetime, with the convention $\epsilon^{01} = +1 = -\epsilon^{10}$, $\epsilon^{11} = \epsilon^{00} = 0$. The corresponding conserved charge for the soliton (kink) solution

$$\begin{aligned} Q &= \int_{-\infty}^{\infty} dx \mathcal{J}^0 = \frac{1}{2} \frac{\sqrt{\lambda}}{m} \int_{-\infty}^{\infty} dx \phi'(x) \\ &= \frac{1}{2} \frac{\sqrt{\lambda}}{m} \left(\phi(+\infty) - \phi(-\infty) \right). \end{aligned} \quad (12)$$

The above relation (12) implies that a constant ϕ solution is, as expected, characterised by a trivial $Q = 0$, but the kink soliton solution is characterised by a non-trivial charge $Q = +1$ ($Q = -1$) for the anti-kink).

Because Q is a constant, the kinks are stable, and never decay to a solution with $Q = 0$, thus Q plays the role of a *topological charge* [10], and the stability of the kink soliton is due to topological reasons. We mention for completion that the topological charge can provide an equivalence-class classification for the various soliton solutions of a field-theory system. Solutions corresponding to the same value of Q belong to the same equivalence class, despite the fact that they may look different in form. The above considerations characterize all types of solitons, even in higher-dimensional field theoretic systems.

The topological stability of these solitons posits intriguing consequences for quantum computation. While the framework is general, we focus it here on the specifics of microtubular networks made of tubulin, microtubule associated proteins, GTP and GDP all inside the highly dynamic aqueous milieu of the cytosol literally bathed in thermal noise of the order of $k_B T = 4.3 \times 10^{-21}$ J or 27 meV at 37° C (or 310° K). We demonstrate how in our mathematical framework loss-less soliton configurations occur and therefore relevant to the development quantum computation out of biologically scalable structures. We use *optimal path* selection (on behalf of the biosystem) as the handle.

While it is true these solitons appear as classical solutions, nonetheless they are the result, of *purely quantum* coherent states, formed in biological systems under physiological conditions. However, due to the complex environment of typically aqueous microenvironment of biological entities, the long-assumed view has been that any quantum effects decohere [13] too quickly to matter for anything actually observable and of biological relevance.

It is true that the conditions necessary for the appearance of coherent states leading to the solitons proposed here are delicately fine-tuned, but that appears to be the unspoken rule of biomolecular interactions in biological systems. From the delicately coordinated balance of enzymatic activity to receptors routinely capable of single-molecule capture and even differentiation between isotopes (a literally *subatomic* feature!) via systems as grossly integrated as the olfactory

sensing and memory apparatus of *Drosophila melanogaster* fruitflies [17, 18] what appears to be incredible odds for a laboratory to achieve can sometimes be commonplace occurrences in biological systems.

At this stage we consider it as important to point out that [19], even if a MT decoheres in a time scale as short as a few hundreds of femtoseconds, this still allows for quantum effects to play a significant role associated with a ‘decision’ on behalf of realistic biological systems on the most optimal path for efficient energy and signal transfer. Indeed, short decoherence times of that order have been shown in [20, 21] to be sufficient for information processing via quantum entanglement at ambient temperatures in *cryptophyte marine algae*.⁴

In these algae, there are eight chromophore antennae (that change their absorption characteristics and therefore colour upon absorbing certain wavelengths) held in place by the protein scaffold creating the light harvesting complexes. The electronic absorption [21] spectrum of this complex system, was elucidated by applying a laser pulse of 25 fs duration. The pulse excites a coherent superposition (in the form of a wave packet) of the antenna’s vibrational-electronic eigenstates. The quantum evolution of such a system of coupled bilin molecules under these initial conditions, predicts that the excitation subsequently oscillates in time between the positions at which the excitation is localized, with distinct correlations and anti-correlations in phase and amplitude. Such coherent oscillations last until the natural eigenstates are restored due to *decoherence*, as a consequence of environmental entanglement [13]. These experimental results [21] confirmed such behaviour, showing a quantum superposition of the electronic structure of the bilin molecule dimer dihydrobiliverdin at room-temperature system lifetimes of order

$$t_{\text{decoh}} = 400 \text{ fs} = 4 \cdot 10^{-13} \text{ s} . \quad (13)$$

The quantum oscillations of these molecules were transmitted to the other bilin molecules in the complex, at distances 20 Angströms apart, ”as if these molecules were connected by springs”. Others have previously [21], concluded that distant molecules within the photosynthetic light harvesting protein complexes are ”*long-range, multipartite quantum entangled even at physiological temperatures*” [23]. Long-lived quantum coherence in the photosynthetic Fenna Matthews-Olson Complex [24] and quantum excitation transport [24] show quantum entanglement surviving over biologically relevant distances creating observable effects in living matter at ambient temperature. This explicitly assigns a critical role to the exclusively quantum phenomenon of entanglement as necessary for the observed path optimization of energy transmission. This has clear implications for quantum computation which we explore in Sections IV-VI below.

Similar arrangements for extreme-quantum efficiency energy transduction have been studied in the context of photosynthesis [23], and have guided attempts at creating artificial leaves [25].

The list of systems found in nature that exploit the toolkit exclusive to quantum physics has grown to include species and settings of such a wide range that it leads us to wonder why we ever failed to expect evolution would be exploiting the availability of quantum trickery -as it can confer significant adaptive advantage such as for instance lossless energy transduction and path optimized transmission finding the most efficient paths over distances of the order of a few nm, spanning several typical protein lengths and highly relevant to receptors and other small-molecule binding biostructures.

The structure of this article is the following: in the next section II, we review the main theoretical pseudospin model of MT [7], which admits various solitonic solutions, among which helicoidal snoidal waves, which will play an important rôle in our analysis, proving a crucial feature for the rôle of MT as quantum (bio)computers. Such a classical pseudispin model is viewed here as a result of a (partial) collapse of a the newtwork of (quantum) tubulin dimr states, as we explain in some detail. In section III we review the rôle of networks of MTs as classical logic gates, giving emphasis on the rôle of solitons, as well as the Microtubule associated proteins (MAP), which provide a crucial connection across different MTs in the newtwork, thus enforcing their rôle as logic gates. In section IV we describe the basic ingredients for the MTs to operate as scalable biocomputers, namely we discuss the basic information storage unit, the relevant quantum-decoherence mechanism, and the “decision-making” process on the most effective path to be followed for a dissipation-free signal and information transduction across the MT. All the above processes take place within the quantum-decoherence time. We provide a microscopic mechanism, within the QED Cavity model of MT [1, 3, 4], which ensures a relatively long decoherence-time interval, allowing for crucial biocomputing processes to take place. The important rôle of the ordered-water interia of the MT in this respect is highlighted. In section V we discuss an experimental-verification path to be followed in order to falsify or, hopefully, verify (!), the above model, thus supporting further the assumption on the potential rôle of MT as quantum (bio)computers. Specifically, we discuss the Rabi splitting phenomenon, which is associated with the rôle of the entire MT as a cavity, and, if verified, would be a strong indication in favour of the model. We also describe experimental arrangements, and the pertinent

⁴ We note, for completeness, that experimental demonstration on the role of quantum effects in biological systems has started becoming available already since since 2007, when research work on photosynthesis in plants [22] has presented rather convincing experimental evidence that light-absorbing molecules in some photosynthetic proteins capture and transfer energy according to *quantum-mechanical probability laws* instead of classical laws at temperatures up to 180° K.

measurements, that would probe quantum coherence and environmental entanglement in individual tubulin dimers, which are the important building blocks of a MT. For the benefit of the reader we summarise our assumptions on the various parameters of the models, and the pertinent physiological conditions, in two tables. Finally, our conclusions and outlook are given in section VI.

II. SOLITONIC EFFECTS IN MICROTUBULES AND OBSERVABLE BIOLOGICAL FUNCTIONS

The role of microtubules (MTs) as candidates for coherent energy or signal transduction has been previously proposed in the context of quantum electrodynamics (QED) models [3, 4]. In light of experimental demonstrations of long-lived quantum coherence in light-harvesting complexes [20, 21, 23, 26], and inspired by efforts to engineer biomimetic systems such as artificial leaves [25], these conjectures warrant renewed theoretical attention [19]. While MTs and algal light-harvesting antennae are structurally and functionally distinct, both are intricate protein assemblies. The observation of robust quantum coherence in biological systems at ambient temperatures provides compelling motivation to consider that analogous mechanisms may underlie energy and information transfer in MTs *in vivo*, consistent with the theoretical framework developed in Refs. [3, 4].

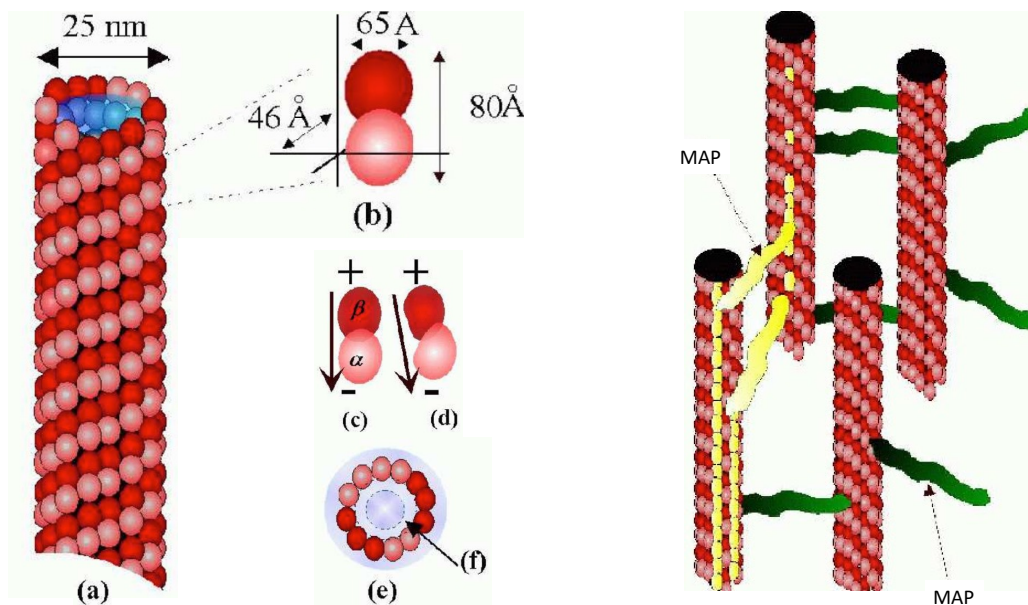


FIG. 3. **Left** : A microtubule (MT) (a), showing individual dimer subunits and their dimensions (b) (1 Angstrom = 0.1 nm). The walls consist of tubulin protein dimers ((c) GTP tubulin, (d) GDP tubulin), which are arranged usually in 12 or 13 helical protofilaments (vertical chain-like structures, parallel to the long axis of MT). The interior (e) is full of ordered water molecules. In the cavity model of MT [1, 3], a thin interior layer near the dimer walls (f) behaves as a high-Q electromagnetic cavity. **Right Picture**: A network of microtubules typical of the neuronal cytoskeleton. The “rungs” cross-connecting MTs are microtubule associated proteins (MAP [17]) (figures from ref. [1])

Basic features of these models are briefly reviewed here in a modern context of quantum computation in connection with biological systems [27–30]. Microenvironmental conditions, for *in vitro* or *in vivo* MT systems, are found to be crucial for the maintenance of the coherence of quantum effects, when the temperature of the system is within physiological parameters.

MTs are fundamental constituents of most eukaryotic cells and all neurons [2], playing a crucial role in the cell structure, growth, shape and mitosis. They have a cylindrical shape and typically consist of 13 (and in some cases 14) protofilaments (see fig. 3). They are formed by the spontaneous polymerization of heterodimers built of two globular proteins (tubulins). The tubulin protein dimers are characterized by two hydrophobic pockets, of length $4 \text{ nm} = 4 \cdot 10^{-9} \text{ m}$ each (the total length of a dimer being $\sim 8 \text{ nm}$ shaped like a peanut in a shell), and they come in two conformations, alpha (α) and beta (β) tubulin, depending on the position of the unpaired electric charge of $18 e$ relative to the pockets, which is responsible for the generation of significant electric dipoles. The internal cylindrical region of the MT (which contains ordered-water [31]) has diameter 15 nm, while the external cross section diameter spans 25 nm.

MTs can grow up to $50 \mu m$ long (with an average length of $25 \mu m$). Each MT is built of a set of macroscopic dipoles which generate dynamical electric fields. The latter prove crucial for an understanding of the functional properties of MTs and their interactions in biological systems.

In [32], the formation of one-spatial dimensional solitons in simplified ferroelectric models of MT has been studied from a rather phenomenological point of view. It has been argued in that work that such solitonic structures, which were assumed propagating along the MT main symmetry axis, provide efficient energy-transfer mechanisms. These solitons are kinks of an appropriate variable, associated with the appropriate projection (on the main MT axis) of the electric dipole displacement vectors between the two tubulin dimer alpha and beta conformations.

In a series of works [3, 4], we have developed a microscopic *quantum electrodynamics cavity model* for MT and proposed phenomenology and experimental pathways towards validation [33]. In our model, we took the full cylindrical structure into account, together with the ordered-water interior of the MT. A crucial role in our construction is played by the strong dipole-dipole interactions between the ordered-water dipole quanta with the electric-dipole moments of the tubulin dimers. These interactions are strongest for water dipole quanta, near the hydrophobic tubulin dimer walls of the MT, in interior cylindrical regions of about 10 Angström from the walls. These electromagnetic dipole-dipole interactions are responsible for overcoming thermal losses and are found [3] to be the dominant forces, leading to environmental entanglement and eventual decoherence à la Zurek [13] in:

$$t_{\text{ow-decoh}} = \mathcal{O}(10^{-6} - 10^{-7}) \text{ s}. \quad (14)$$

It is important to stress once again at this point that such a decoherence time is due exclusively to the rôle of the ordered water in the MT interiors, specifically it is assumed in [3] that the main source of decoherence is the loss of ordered-water dipole quanta through the imperfect MT cavity walls, made out of tubulin dimers. The decoherence time (14) is much longer than, e.g. the one advocated in the analysis of [34], where the approach of [15] to consciousness has been criticized), of order in the range $t_{\text{decoh MT estimate}} \in 10^{-20} - 10^{-13}$ s, depending on the specific environmental source. The upper limit of this short decoherence time has been considered in [34] as a conservative estimate, corresponding to the case in which the main decoherence-source are the Ca^{2+} ions in each of the 13 MT protofilaments. Although, for reasons stated, we disagree that such a short decoherence time applies to the QED cavity model of MT [3, 4], nonetheless we point out that such short decoherence times are not far from the decoherence times (13), which proved sufficient for the Algae antennae to quantum compute the optimal path for information transduction across distances of order 2.5 nm. As we shall argue below, such short decoherence times might also be sufficient for a ‘decision making’ process on behalf of basic groups of heterodimers in a MT which may constitute the unit of quantum computation (qu(D)it), see discussion below in section IV in such systems.

The basic underlying mechanism for dissipation-free energy and signal transduction along the MT is the formation of appropriate *solitonic* dipole states in the protein dimer walls of the MT, which are reminiscent of the quantum coherent states in the Fröhlich-Davydov approach. These dipoles states are classical, obtained after decoherence of quantum states, and correspond to solutions of the non-linear equations that describe the dynamics of the MT within certain models that take proper account of the dipole-dipole interactions.

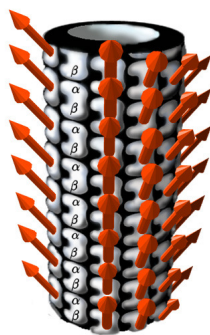


FIG. 4. The structure of the cytoskeleton microtubule (MT). The arrows indicate the orientation of the permanent dipole moments of the tubulin heterodimers with respect to the MT surface. The permanent dipole moments of the tubulin dimers are all oriented in such a way that the spherical polar angle of the dipole vectors with respect to the symmetry axis of the MT (assumed here along the z direction) is approximately [35] $\Theta_0 \simeq 29^\circ$. Picture from ref. [7].

In this respect, in ref. [7], we have discussed the emergence of, and classified, various kinds of solitonic excitations, which arise as solutions of the field equations of appropriate classical field theoretic non-linear systems that model the MT dipole interactions in the tubulin dimer. We have used the full cylindrical geometry of MT, but we did not take

into account the complicated ordered-water interior, whose role as mentioned above, was assumed simply to provide -through its dipole interactions with the tubulin dipoles - the long decoherence time (14). So although important in this latter respect, the role of the ordered water was not considered further in [7], where we constructed a classical non-linear pseudospin σ -model, which we assumed to describe the coherent (classically behaving) state of the tubulin dipole quanta after the elapse of the decoherence time (14) (see fig. 4). As discussed in the relevant literature [35], in the ground state of an MT, the orientation of the permanent dipole moments of the tubulin dipoles with respect to the surface of the MT is such that the relative spherical polar angle with the symmetry axis of the MT is $\Theta_0 \approx 29^\circ$. We suggest here that, during the decoherence time (14) (or even in shorter time intervals), in analogy with the situation in Algae, the MT “quantum computes” the most efficient pathway for energy transfer, which is realized by the formation of the appropriate solitons, in the way we describe below.

As discussed in [7], due to their interaction with the noisy aqueous microenvironment, MTs can experience a strong radial electrostatic field leading to the additional (radial) polarization of tubulins [36], as happens, for instance, in the wake of a biomolecular binding event or passage of an action potential. In such cases, it is known that, even inside brain-MT bundles, fields such as those generated by passing action potentials can be felt, and the associated electrical oscillations have been observed experimentally [37]) The total mass of each tubulin heterodimer can be estimated as, ($M \approx 1.84 \cdot 10^{-19}\text{g}$). Each heterodimer can be considered as effective electric dipole with α and β tubulin being as positive and negative side of the dipole, respectively [38].

In the model of [7], each dipole is treated as a classical pseudo-spin, \mathbf{S}_i , with a constant modulus. The lattice model (over the lattice of the dimers) describes the dynamics of tubulin dipoles and their interactions across the two-dimensional MT cylindrical surface. The potential energy of the system can be written as [7]:

$$U = S^2 \sum_{\langle i,j \rangle} J_{ij} (\mathbf{n}_i \cdot \mathbf{n}_j - 3(\mathbf{n}_i \cdot \mathbf{e}_{ij})(\mathbf{n}_j \cdot \mathbf{e}_{ij})) + \sum_i (PS^2(\mathbf{n}_i \cdot \mathbf{e}_z)^2 + QS^4(\mathbf{n}_i \cdot \mathbf{e}_z)^4 - BS\mathbf{n}_i \cdot \mathbf{e}_r). \quad (15)$$

where we have parameterized the pseudo-spin \mathbf{S}_i by the unit vector \mathbf{n}_i , as: $\mathbf{S}_i = S\mathbf{n}_i$, where S is the module of \mathbf{S}_i , assumed constant in our approach, as already mentioned. In [7], we took the direction along the z spatial axis to coincide with the main symmetry axis of the MT. The quantity \mathbf{e}_{ij} denotes the unit vector parallel to the line connecting the dipoles, the latter being represented by the pseudospin vectors \mathbf{S}_i and \mathbf{S}_j . The first term on the right-hand side of (15) describes the dipole-dipole interaction among the tubulin dimers. The pertinent interaction coupling J_{ij} depends on the inverse cubic power of the distance between dipoles, according to the well-known law of electrostatics,

$$J_{ij} = \frac{1}{4\pi\epsilon\epsilon_0 r_{ij}^3}, \quad (16)$$

where ϵ is the permittivity of the MT microenvironment in units of that of the vacuum, ϵ_0 , and r_{ij} is the distance between sites i and j of the lattice model. As is common, in [7] we assumed that J_{ij} , are nonzero only for the nearest-neighbor dipole moments (in practice, next to nearest neighbor dipole-dipole interactions are considered suppressed). The middle term, with P and Q appropriate interaction couplings, has the form of a double-well quartic on-site potential, and takes into account [39] the assumed ferroelectric properties at physiological temperature ranges for the MT [35, 40], and their effects on the effective spin, \mathbf{S}_i , while the last term, describes the effects of the transversal (radial) electrostatic field with amplitude B acting on the dipoles, which is produced by the solvent environment of the MT. Thus, all the further effects of the ordered water molecules (apart from their important contribution to lead to the long decoherence time (14)), are captured by this term.

The system of MT dimers may be represented as a triangular lattice, as shown in Fig. 5, so that each spin has six nearest neighbors. The constants of interaction between the central dipole (labelled “0”) in Fig. 5 and its nearest neighbors are denoted as $J_{0\alpha}$, and the distance between the central spin and its nearest neighbors as d_α ($\alpha = 1, 2, \dots, 6$). We set $d_{01} = d_{04} = a$, $d_{02} = d_{05} = b$, $d_{03} = d_{06} = c$. The corresponding angles (between the central dimer and others) are denoted as, θ_1 , θ_2 and θ_3 , so that: $\mathbf{e}_{01} \cdot \mathbf{e}_{01} = \cos \theta_1$, $\mathbf{e}_{01} \cdot \mathbf{e}_{02} = \cos \theta_2$, $\mathbf{e}_{01} \cdot \mathbf{e}_{06} = \cos \theta_3$. Typical values of parameters known from the literature are: $a = 8 \text{ nm}$, $b = 5.87 \text{ nm}$, $c = 7.02 \text{ nm}$, $\theta_1 = 0$, $\theta_2 = 58.2^\circ$, $\theta_3 = 45.58^\circ$, $S = 1714 \text{ Debye}$ [39, 41] (See Fig. 5b.) The radius of the MT can be estimated as, $R \approx 11.2 \text{ nm}$ [35, 42]. The unit cell shown in Fig. 5 consists of the central spin surrounded by six neighbors. Its area is: $\Sigma_0 = 3ad = 120 \text{ nm}^2$.

As discussed in [7], the continuum approximation proved sufficient for classifying and studying the solitonic solutions arising from the non-linear lagrangian corresponding to the pseudospin non-linear σ -model with interaction potential given by (15). Using the local spherical coordinates (Θ_i, Φ_i) to define the orientation of the dipole,

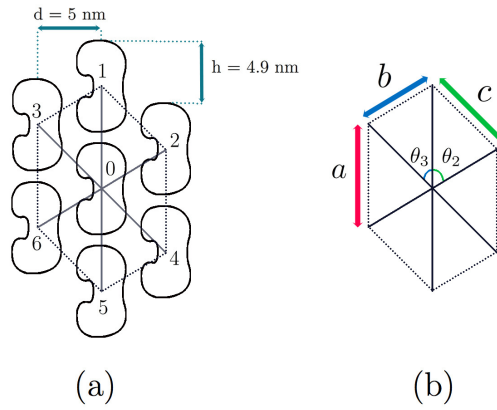


FIG. 5. Tubulin neighborhood in the hexagonal unit cell of the microtubule. The distance between dimers is d . The heterodimer helix direction is defined by the height, h . The typical values of parameters are: $a = 8$ nm, $b = 5.87$ nm, $c = 7.02$ nm, $d = 5$ nm, $h = 4.9$ nm, $\theta_1 = 0$, $\theta_2 = 58.2^\circ$, $\theta_3 = 45.58^\circ$ [35, 39, 41, 42]. This structure will play the rôle of the quDit basic information storage unit in our modelling of the MT as a biocomputer.

$\mathbf{n} = (\sin \Theta \cos \Phi, \sin \Theta \sin \Phi, \cos \Theta)$, then, the continuum Lagrangian of the system reads:

$$\begin{aligned} \mathcal{L} = & \frac{\rho}{2} ((\partial_t \Theta)^2 + \sin^2 \Theta (\partial_t \Phi)^2) + \frac{1}{2} ((\nabla \Theta)^2 + (\nabla \Phi)^2) \\ & - \frac{h}{2} (\cos \Theta \sin \Phi \nabla \Theta + \sin \Theta \cos \Phi \nabla \Phi)^2 - \frac{h}{2} \sin^2 \Theta (\nabla \Theta)^2 - \mathcal{W}(\Theta, \Phi), \end{aligned} \quad (17)$$

with the interaction potential $\mathcal{W}(\Theta, \Phi)$ assuming the form [7]

$$\begin{aligned} \mathcal{W}(\Theta, \Phi) = & (g_0 - h) \cos^2 \Theta \\ & + g_1 \cos^4 \Theta - h \sin^2 \Theta \sin^2 \Phi - g_2 \sin \Theta \cos \Phi, \end{aligned} \quad (18)$$

with $h = (6S^2/J) \sum_{a=1}^3 J_{0a} \cos^2 \theta_a$, $g_0 = PS^2/J$, $g_1 = QS^4/J$, $g_2 = BS/J$, and $J = 2S^2 \sum_a^3 J_{0a}$. On introducing the dimensionless coordinates, $\zeta = z/\sqrt{\Sigma_0}$ and $\tilde{R} = R/\sqrt{\Sigma_0}$, the continuum Lagrangian of the system becomes that of an anisotropic σ -model:

$$\mathcal{L} = \frac{\rho}{2} \left(\frac{\partial \mathbf{n}}{\partial t} \right)^2 + \frac{1}{2} (\nabla \mathbf{n})^2 - \frac{h}{2} (\nabla n^2 \cdot \nabla n^2 + \nabla n^3 \cdot \nabla n^3) - \mathcal{W}(\mathbf{n}), \quad (19)$$

with $\mathcal{W}(\mathbf{n}) = h(n^1)^2 + g_0(n^3)^2 + g_1(n^3)^4 - g_2 n^1$, with the order parameter, \mathbf{n} being the local polarization unit vector specified by a point on the pseudospin sphere, S^2 .

In [7] the zero-temperature phase diagram of this model has been studied in detail, yielding for the ground state (which is characterized by a permanent dipole moment) a paraelectric and a ferroelectric phase, separated by the line $\kappa = 4\sigma$, where $\sigma \equiv (h - g_0)/(2g_1)$ and $\kappa \equiv g_2/g_1$. The ferroelectric phase of the MT ground state occurs for $\sigma > 0$ and $\kappa = g_2/g_1 < 4\sigma$, while the paraelectric phase occurs in the regime of parameters $\sigma < 0$, and $\kappa > 4\sigma$. This zero-temperature paraelectric phase corresponds to the radial orientation of the permanent dipole moments of the tubulin dimers with respect to the surface of the MT. For finite temperatures of interest to realistic MT systems, we refer the reader to [43] where the critical order-disorder transition temperature depends on the values of the dipole moment and the electric permittivity of the system. It will not be of further impact to our considerations in this paper. We only remark for completion that a discussion on the importance of ferroelectricity in biological systems has been given in [44], and it has been at the heart of the concrete MT modelling since the early days [32], [3].

The classification of the (finite energy) soliton solutions of the Lagrangian system (17) is of interest, and as discussed in [7], there are kink, snoidal waves, spikes and helicoidal static soliton and also waves propagating along the MT. Of specific relevance to our case are the helicoidal waves due to their stability, but also due to the general applicability of such helical structure models to many scales and sizes in biology from the alpha helices and chirality of small signaling molecules to the ubiquitous helices of DNA and RNA and their numerous variants in most chiral biopolymers. In order to construct solutions of the equations of motion for nonlinear waves moving along the MT with a constant velocity, v , we use the traveling wave ansatz. We assume that in cylindrical coordinates the field variables are functions of

$$\xi = \sqrt{\frac{2}{\eta p \Sigma_0}} (z + h_0 \varphi / 2\pi - vt), \quad (20)$$

where $\eta = h/g_1$ and $p = 1 + (h_0/2\pi R)^2$. On defining $u = \cos \Theta$, one can then show that the field equations possess the first integral of motion [7]:

$$\begin{aligned} & (u_0^2 - \cos^2 \Theta) \left(\frac{d\Theta}{d\xi} \right)^2 + \sin^2 \Theta \left(u_0^2 - \frac{1}{h} \cot \Theta - \sin^2 \Phi \right) \left(\frac{d\Phi}{d\xi} \right)^2 \\ & + \frac{1}{2} \sin(2\Theta) \sin(2\Phi) \frac{d\Theta}{d\xi} \frac{d\Phi}{d\xi} - (\sigma - \cos^2 \Theta)^2 + \eta \sin^2 \Theta \sin^2 \Phi + \kappa \sin \Theta \cos \Phi = \text{const}, \end{aligned} \quad (21)$$

where $u_0^2 = 1 - 1/h - \rho v^2/(hp\Sigma_0)$. This implies for the nonlinear wave propagation velocity v :

$$v = \sqrt{(\sigma_0^2 - u_0^2) \frac{hp\Sigma_0}{\rho}}, \quad (22)$$

where we set $\sigma_0^2 = 1 - 1/h$. For completeness, we mention that the analysis of [7], taking into account the parameters entering the model of MT under consideration here, shows that dependence of v on the parameter that the velocity of the wave is bounded from above $v \leq v_0$, where $v_0 \approx 155\text{m/s}$.

There are *one-dimensional solutions* characterised by $\Phi = 0$, which propagate along the symmetry axis of the MT, in similar fashion to the one-dimensional solitons of the initial simplified models of MT [3, 4, 32]. In that case, we choose for convenience the constant of integration on the right-hand-side of eq. (21) (upon setting $\Phi = 0$) as $\varepsilon = (\sigma - u_0)^2$. We then observe that the solutions are snoidal waves and kinks, corresponding to the case where $\kappa = 0$, which implies the absence of the intrinsic electric field ($g_2 = 0$).

The solution corresponding to a snoidal wave, is given by the following expression:

$$u = k \text{sn}(\xi - \xi_0, k). \quad (23)$$

Here $k = \sqrt{2\sigma - u_0^2}$, and $\text{sn}(z, k)$, $z \in \mathbb{C}$, is the Jacobi elliptic function [45]. Hence, the sn waves exist when $u_0^2 < 2\sigma < 1 + u_0^2$. The period T of the sn-wave is proportional to the complete elliptic integral of the first kind [45]:

$$T = 4 \int_0^{\pi/2} \frac{d\varphi}{\sqrt{1 - k^2 \sin^2 \varphi}}. \quad (24)$$

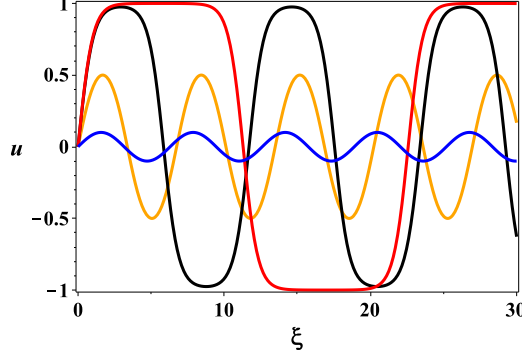


FIG. 6. The sn-solution: $k = 0.1$ (blue), $k = 0.5$ (orange), $k = 0.975$ (black), $k = 0.9999$ (red). Picture taken from [7].

The static sn-solutions for different choices of the constant k are depicted in Fig. 6 [7]. For $k^2 \ll 1$ and $k'^2 = 1 - k^2 \ll 1$. It can be seen [7] that the solutions go to zero smoothly $u \rightarrow 0$, as $k, k' \rightarrow 0$, whilst when $k = 1$ the sn-waves become the *kink* (cf. (7)):

$$u = \tanh(\xi - \xi_0), \quad (25)$$

with the boundary conditions: $u(\pm\infty) = \pm 1$.⁵

⁵ Kinks, as is well known [10, 46], and discussed in the introduction of this article, admit a topological classification in terms of the appropriate homotopy group. In our case, the topological charge, π_0 , of the kink (7) is determined by the magnitude, n_z of the polarization vector at the ends of the MT:

$$\pi_0 = \frac{1}{2}(n_z(+\infty) - n_z(-\infty)). \quad (26)$$

To change the topological charge one needs to overcome the potential barrier, proportional to the size of the MT (formally, infinite potential barrier).

We remark at this point that such one-dimensional solitons have been considered in connection with dissipation-free energy and signal transduction in phenomenological one-dimensional models of MT in [3, 32]. In [7], such solutions have been derived from realistic three-dimensional lattice models, entailing dipole-dipole interactions on the dimer walls of a MT.

Apart from kinks, another interesting solution for the case $\kappa = 0$ are *Spikes*. The latter are excitations of the ground state. Estimates of the energy carried by a spike have been provided in the analysis of [7]. The electric field produced by the spike can be estimated as [7], $\Delta E_z = E_z^{\max}(u_{sp}^2 - u_g^2)^2$, where $E_z^{\max} = \frac{Jg_1}{S}$ is the maximum value of the electric field due to the permanent dipoles, which is reached when all dipoles are aligned along the MT (in which $u_g = 1$). The maximum value of the electric field produced by spike $\Delta E_z \leq \Delta E_z^{\max}$, has been estimated in [7] as $\Delta E_z^{\max} = E_z^{\max}(1 - u_g^2)^2 = E_z^{\max} \cos^4 \Theta_0 \leq E_z^{\max}$, where Θ_0 denotes the angle between the permanent dipole and axis orthogonal to the surface of the MT. Notice that the maximum magnitude of the electric field produced by spike is bounded by E_z^{\max} . As discussed in the literature [35], and mentioned above, in the ground state the orientation of the dipoles with respect to the surface of the MT are $\Theta_0 \approx 29^\circ$. Taking into account data from [7], one can arrive at the following estimation for the electric field produced by the spike: $\Delta E_z^{\max} \approx 0.6E_z^{\max}$. To evaluate E_z^{\max} , we use data available for the electric field inside of the MT: $E_z \sim 10^5 \div 10^8$ V/m [32]. Then, we arrive at the following estimate for the electric field produced by the spike: $\Delta E_z^{\max} \lesssim 0.6 \cdot (10^5 \div 10^8)$ V/m.

In addition to solutions with $\Phi = 0$, there are also solitonic configurations with $\Theta = \frac{\pi}{2}$, $\Phi \neq 0$, which are chiral solitons that are related to the paraelectric ground state. Finally, there are also two-dimensional solutions, with both $\Phi \neq 0, \Theta \neq 0$, which have the form $\Theta = \Theta(z + \nu\varphi - vt)$ and $\Phi = \Phi(z + \nu\varphi - vt)$. Such solutions describe two-dimensional nonlinear waves propagating on the MT surface along the z -direction. Among the solutions, are two-dimensional kinks, static helicoidal snoidal solutions, and a *helicoidal sn-wave*, which is of central interest to our discussion here. For details we refer the reader to [7]. In fact, there could be travelling helicoidal solitonic solutions combined to a double helix along a MT, mimicking the structure of DNA molecules, which are known to be particularly stable [47].

In our picture, as already stressed, we view the above classical solutions as various outcomes of coherent superposition of quantum states of dipoles.

III. MICROTUBULAR NETWORKS AS LOGIC GATES

Above we have reviewed work on soliton solutions arising in the non-linear dynamics of dimer dipoles in microtubular biosystems modelled by pseudo spin non-linear σ -models. The presence of such solitons, if confirmed by Experiment [48], would serve as a critical step towards our understanding of energy and signal transduction by (these) biological entities.

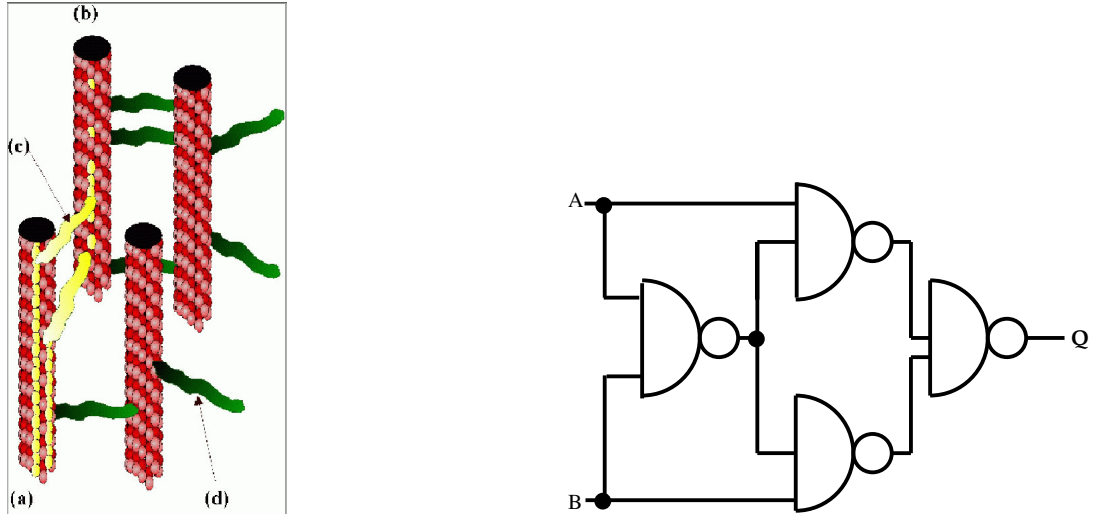


FIG. 7. A MT arrangement in cell as a ‘logic’ XOR gate. Left panel: the biological arrangement, a group of MTs and their MAPs, reproduced from [1]. Right panel: a conventional XOR gate for comparison.

In addition to efficient energy transport, the presence of solitonic structures in MT may imply their role as biological

logic gates, as proposed initially in [4], and elaborated further, from a quantum computational viewpoint in [1] (See fig. 7, left panel). Although MT do not themselves branch, the analogue of a ‘logic’ XOR gate (see Fig. 7, right panel) by MT arrangements in cells has been proposed with microtubule associated proteins (MAPs) that connect the various MTs in a network given the role of information storage [17, 18, 33]. Once a soliton is formed along one MT, an “active MAP” (yellow colour in left panel of Fig. 7) can transport it from one MT to another. In the MT arrangement depicted on the left panel of Fig. 7, an XOR logic gate can be realized provided the “0” entry is represented by the absence of a soliton and the “1” entry by the presence of a soliton. In this arrangement, MT (a) acts as the “Input” MT, whilst MT (b) is the “Output” MT. (c) is a MAP transmitting a soliton, while (d) represents a “quiet” MAP (green coloured MAPs). MT (a) has two solitons travelling (yellow colour), encountering two MAPs (yellow coloured MAPs) that transmit both solitons to MT (b). The solitons would arrive out of phase at MT (b) and cancel each other out. The truth table for XOR reads: $0, 0 \rightarrow 0$; $0, 1 \rightarrow 1$; $1, 0 \rightarrow 1$; $1, 1 \rightarrow 0$, and in this case is realized by MTs if the MAPs are arranged in such a way that each can transmit a soliton independently but if they both transmit, then the two solitons cancel each other out. We stress that the existence of snoidal waves is crucial for the behaviour of MT as logical gates, since for such solitonic structures, the out-of-phase cancellation $1, 1 \rightarrow 0$ exists automatically.

IV. SCALABLE QUANTUM COMPUTATION IN MICROTUBULES

A scalable quantum system is defined as the one that can grow from a few qubits to thousands or even millions, while maintaining its performance before the scaling. Sometimes this may require an integration with some classical computing resources. In this section we shall attempt to address this question with reference to the Microtubules, which we shall argue can behave like scalable quantum computers, under some circumstances that we shall specify. In fact, as we shall argue below, the basic storage information unit of an MT when viewed as a quantum coherent system is a quDit, that is, a higher-dimension qubit [29, 49]. To have a complete mapping of any system into a quantum computing device, the following important issues should be addressed [50]: (i) a precise description of the quantum states of the basic information storage unit (qubit or quDit), (ii) a description of the mechanism through which the wavefunctions representing these states become entangled, including specification of the basis in which measurements of the qub(D)it’s properties are performed in situ, and (iii) a means of achieving quantum coherence over the required time scale. It is the purpose of this section to address such questions and present a consistent model of MT as a quantum biocomputer.

To this end, we first remark that above we have treated the solitons on a MT as classical solutions, and the XOR gate role of MT arrangements was construed according to classical physics and computation. As in our previously published work [3, 4], these solitons are treated as *macroscopic quantum coherent states*, or at most as (not completely decohered, minimum entropy) pointer states [16], which survive long enough so that processes such as energy transmission (and by extension memory storage) along MTs of length of a few μm are allowed to take place. In our approach, this can happen under fine-tuned conditions [3], that defend the system from environmental decoherence losses. The dipole-dipole interactions between the tubulin dimers and ordered-water dipole quanta [51] in the neighborhood of the (hydrophobic) walls of the MT tubulin dimers are crucial in accomplishing this.

A. Proposed mechanisms for biocomputation: dipole-dipole interactions between MT dimers, water microenvironment and external fields

At a quantum level, these dipole-dipole interactions of a tubulin dimer with dipole \vec{p} and its fluid environment can be expressed via interactions of the form (15), (16), where the S_i now are viewed as components of a quantum spin (pertaining to the dimer and the ordered-water dipole quantum) and not a pseudospin as in the classical model of [7], discussed in section II above. For concreteness, the relevant interactions between tubulin dimer (TD) and ordered-water dipoles (OW) read schematically:

$$U \ni \sum_{i \neq j} \frac{1}{4\pi \epsilon_0 r_{ij}^3} \widehat{S}_i^{\text{TD}} \cdot \widehat{S}_j^{\text{OW}}, \quad (27)$$

where now $\widehat{S}_{i,j}^{\text{TD,OW}}$ are quantum operators corresponding to spin vectors, and ϵ represents an average permittivity (in units of the vacuum permittivity ϵ_0) of the MT microenvironment including the ordered-water interior. In view of its cubic scaling power with the distance between dipoles (the dominant interactions, as expounded upon in [3]), which are strong enough to overcome thermal losses at room temperatures, are those in a region near the dimer walls, of small thickness 20 Angstroms. This provides an analogy of the MT as isolated, high-quality QED cavities [3], and lead

to decoherence times of order given in (14). The quality factor of the cavity depends crucially on the strength of the interaction (27), which also involve the dependence on the permittivity parameter ε . The smaller the ε , the stronger the dipole-dipole interactions, and thus the longer the decoherence time of the system of tubulin dimers, before its collapse to one of the solitonic states [7] discussed in section II, most likely, from the point of view of stability, to the double helix as we shall discuss below.

We remark at this point that in the *ferroelectric phase* of the system of the tubulin dimers [3, 7, 52], ε may increase significantly compared to its value in normal non-ferroelectric environments, especially at temperatures near the critical temperature of the pertinent phase transition. In principle this would have an effect in shortening the decoherence times, especially in room temperatures, which is supposed to be the order of the critical temperature of the MT systems viewed as ferroelectric/ferrodistortive ones [3, 7, 52]. In the approach of [3], this effect is compensated by the presence of the thin regions near the dimer walls where the ordered-water-tubulin-dimer interactions (27) become very strong, due to the r_{ij}^{-3} scaling.

In a different setting than the QED-Cavity MT model of [3], the authors of [53], consider the mean-field electromagnetic (Coulombic) interaction between a single-tubulin-dimer dipole moment \mathbf{p} and the net electric charges, of density $\rho(\mathbf{r})$, in its aqueous cellular environment as the main source of decoherence. Such an interaction arises from the net (positive and negative) electric charges at the surface of a dimer, which via Debye shielding, cause the formation of a *counterion* layer, on top of the dimer-surface charged layer. This counterion layer contains unpaired (positive and negative) charges and electrically neutral (mainly water) molecules. In [53] it was assumed that the cellular environment behaves as a plasma, characterised by a Debye length λ_D and plasma frequency ω_p , which describes the collective oscillations of ions. The counterion layer has a thickness of order λ_D . The plasma-like cellular environment of the MTs contains quantum excitations of the charge density (plasmons). When these plasmons are in an excited state, the electrical neutrality of the cellular aqueous environment of the tubulin dimers is destroyed, and net charges appear.

These charges interact electromagnetically (via Coulomb forces) with the dimer dipole, leading to a contribution to the Hamiltonian of the system of the form:

$$\mathcal{H}_{\text{dipole-environ}} = \int d^3\mathbf{r}' \rho(\mathbf{r}) \frac{\mathbf{p} \cdot \mathbf{r}'}{4\pi \varepsilon \varepsilon_0 |\mathbf{r}'|^3}, \quad (28)$$

where bold face quantities denote three vectors. The authors of [53], as in [3], assumed that $\varepsilon \varepsilon_0 \sim 80$ (the dielectric constant of water at room temperature). This approach is different also from that found in [34], where the cellular environment of the dimers of a MT has been unrealistically simulated by a single distant ion. Nonetheless, even in the more detailed approach of [53], the decoherence time of a tubulin dimer, resulting from the interaction (28), lies in the range

$$t_{\text{dimer-environ}} \in (1, 100) \text{ fs}, \quad (29)$$

which is much shorter than the corresponding decoherence time in the QED-cavity model of [3], (14). The two-orders-of-magnitude uncertainty in the value of $t_{\text{dimer-environ}}$ in (29) are attributed to the corresponding uncertainties of various parameters of the model, including the consideration of ε in the range (24, 240), in the phenomenological analysis of [53]. We note that the upper limit of such decoherence times are not far from the ones established by experimental observations in Algae [21], (13).

The analyses of [53] and [34], ignore the important role of the ordered-water dipole quanta [51]. As we have discussed in [3] and mentioned briefly above, in the thin regions near the dimer walls of the MT, there are strong dipole-dipole interactions of water dipole quanta with the dipole quanta of the tubulin dimers, (27), which overcome/shield the interaction (28) and lead to the behaviour of MTs as high-quality QED cavities, resulting in much longer decoherence times (14), since the basic assumption of the cavity model for MT is that environmental decoherence occurs mainly due to leakage of ordered-water dipole quanta from the MT dimer walls [3] (we discuss briefly some experimental aspects of the model in section V A).

Following [3], we assume that the temperature T of the system of MTs we consider is in the range of room temperatures, e.g. $T = \mathcal{O}(300)$ K, while the permittivity appearing in (27), $\varepsilon \simeq 80$, that is, of order of the dielectric constant of water.

An information manipulation system based on tubulin dipole quanta as the substrate for bioqubits could also provide the basic substrate for quantum information processing inside a (not exclusively neural) cell or lab-borne microfluidic arrangement. In a typical MT network, there may be of the order of 10^{12} tubulin dimers. A question arises as to whether such large aggregates of “subunits” could be quantum entangled, with the entangled state being maintained for a usefully long time. This question has been answered in the affirmative at least in atomic physics, where experiments [54] have demonstrated the existence of long-lived entangled states of *macroscopic* populations of Cs gas samples, each sample containing 10^{12} atoms, or in liquid-state quantum computing experiments [55],

where entanglement among even larger populations of appropriate subunits is generated via interaction with the electromagnetic field at various frequencies.

B. Microtubules as Quantum Computers: Detailed Scheme

One of the basic questions in quantum computation concerns the nature of the basic unit, the qubit or potential higher-(D)-“dimensional” extensions thereof (quDit [29]). We argue below that such a basic quDit is provided by the basic hexagonal cell (*cf.* Fig. 5) of the tubulin dimer (distorted honeycomb) lattice in an MT.⁶

This is to be contrasted with the initial quantum picture of MT’s in [15], in which one views the tubulin dimer conformations as providing quantum states $|0\rangle$ or $|1\rangle$, corresponding to the α or β conformations [15]. The latter are viewed as *identical* for all the dimers, hence the macroscopic coherence in such a system originates from the *orchestrated reduction* [15] of the collective wave-functions of the “identical” dimers, each viewed as a two-state quantum system. However, upon taking into account the environment of the unpaired charges in each tubulin dimer, and the associated physiological, as well as geometrical, differences among the dimers, as indicated by the various parameters in fig. 5(b), one is tempted to assign internal degrees of freedom to the various dimers of the fundamental hexagonal cell. In this viewpoint, therefore, the appropriate formalism to describe the basic unit for storage information, and hence for quantum computation in an MT, would not be a binary qubit system, but a higher-dimension quDit [29, 49]. The number of the independent quantum states actually included in a primary cell such as that depicted in fig. 5 depends on whether there is a symmetry under reflection (*i.e.* rotation of the cell by an angle π).

In the depiction of the dipoles in the present work, we only consider as differences the geometrical characteristic of the individual dipoles, due to the difference in the angles θ_1, θ_2 . Thus, the upper three nearest-neighbour states, labeled as 1,2,3 in fig. 5(a), are treated as identical to the lower ones, 4,5,6. Hence, the independent quantum basis quDit dimer states are the ones at the four vertices of the parallelogram enclosed by the sides b and c , which are labeled as 0,1,2,3, referring to the corresponding dimers in fig. 5(a).

Each of these states is a quantum coherent superposition of α and β conformations, but they are distinct due to their “internal” degrees of freedom. Our (pseudo)spin model [7] is ideal to provide the fundamental unit for storage of information in case one views the MT network as a quantum computer. The reader should recall at this point that QuDit and spin systems go hand in hand [59].

Therefore, in each fundamental parallelogram of the fundamental cell of fig. 5(b), say 0312, where the vertices $i = 0, 1, 2, 3$ label the nearest neighbours of tubulin dimers depicted in fig. 5(a), one encounters a quDit comprised of four-qubit entangled states [60] (since each tubulin-dimer quantum state, before its collapse, can be in a superposition of an α and a β conformations). The four-qubit entangled states of tubulin dimers constitute a convenient basis for the description of the various entangled quDit states in our MT Lattice model (such a basis of four qubits consists of $2^4=16$ Quantum states):

$$\begin{aligned} |\psi^{4 \text{ qubits}}\rangle = & a_0|\alpha\alpha\alpha\alpha\rangle + a_1|\alpha\alpha\alpha\beta\rangle + a_2|\alpha\alpha\beta\alpha\rangle + a_3|\alpha\beta\alpha\alpha\rangle + a_4|\beta\alpha\alpha\alpha\rangle \\ & + a_{12}|\alpha\alpha\beta\beta\rangle + a_{13}|\alpha\beta\alpha\beta\rangle + a_{14}|\beta\alpha\alpha\beta\rangle + a_{23}|\alpha\beta\beta\alpha\rangle + a_{24}|\beta\alpha\beta\alpha\rangle + a_{34}|\beta\beta\alpha\alpha\rangle \\ & + a_{123}|\alpha\beta\beta\beta\rangle + a_{124}|\beta\alpha\beta\beta\rangle + a_{134}|\beta\beta\alpha\beta\rangle + a_{234}|\beta\beta\beta\alpha\rangle + a_{1234}|\beta\beta\beta\beta\rangle, \end{aligned} \quad (30)$$

where the coefficients are in general complex numbers, with the constraint that they lead to appropriate normalization of the state $|\psi^{4 \text{ qubits}}\rangle$. As discussed in [60], such entangled four-qubit states can be used to provide the area of the two-dimensional fundamental parallelogram, which can be constructed from the specific entangled state

$$|\mathcal{A}\rangle = |\alpha\beta\alpha\beta\rangle - |\beta\alpha\beta\alpha\rangle$$

corresponding to a specific quantum circuit, described explicitly in [60].

In the realistic MT case, where the environment of the tubulin heterodimers is taken into account, the two parallelograms of the fundamental MT lattice cell may be inequivalent, as we have mentioned above. In such a case, one has a more complicated quDit structure, since the fundamental storage of information unit now comprises of the two parallelograms 0321 and 0456 (see fig. 5). We leave for future works a detailed exploration of the full potential of the honeycomb MT lattice architecture and the corresponding MT networks, discussed here, for quantum (bio)computation.⁷

⁶ We remark at this point that honeycomb lattices are also the basic structure of the Carbon nanotubes (CNT) [56], which can be thought of as sheets of graphene [57] rolled up in a cylinder. These systems have remarkable structural stability, and an extraordinary combination of mechanical, thermal and electrical properties, including superconducting behaviour, which imply their great potential as energy harvesting and storage devices. We may draw several analogies between CNT and MT, as far as their geometric characteristics are concerned (we also mention that recently graphene layers have been used recently in quantum computation [58]).

⁷ We cannot resist in pointing out, at this stage, that the rôle of the hexagonal MT Lattice fundamental unit in providing a sort of coding for the function of MTs as information storage and processing devices has been pointed out in [61], as discussed by Nanopoulos in [5]. However, as argued in the current paper, it is the entangled states of the two parallelograms of the fundamental hexagonal cell (*cf.* fig. 5) that play a crucial rôle as fundamental information-storage and “decision-making” units, for efficient information and signal transduction across the MT. This type of entanglement also leads to the formation of the double helical solitonic structures of quantum dipoles, which after collapse become double-helix-like snoidal solitonic waves [7], that are mechanically stable, as in the DNA case [47].

These quantum states are quantum entangled (“wired dissipationlessly”) during the time interval (14) (measured from the moment of the action of an external stimulus to the MT), in much the same way as the bilin molecules of the algae antennae. In algae, such a coherent wiring / yoking / quantum entanglement occurs over distances of 25 nm, and the decoherence time is a few hundreds fs. This is evidently sufficient time for the algae molecule to quantum-compute the optimal path for signal transmission over distances covering half of the extent of the algae light harvesting antenna. In the case of the MT, the distances, over which entanglement is expected to survive, are not restricted only to the fundamental cell depicted in fig. 5, but, over the entire MT of lengths of $\mathcal{O}(\mu\text{m})$. This feature is a consequence of the strong dipole-dipole interactions between nearest tubulin neighbours, and also the ordered-water dipole quanta [3, 51] and the tubulin dimers themselves, which provide a stronger isolation than in the case of algae, thus leading to much longer coherence times (14). Indeed, the reader should notice that, if the snoidal waves propagate with a velocity of order at most 155 m/s, as discussed after (22), then signals are transduced across a micron (μm)-long MT in times $\mathcal{O}(10^{-8})$ s, which lies comfortably in the aforementioned decoherence time interval of the QED-cavity model of MT [3].

This allows for quantum computation of the system of dimer dipole quanta in an MT, involving a “decision making process” for determining the optimal path for signal transduction along the MT. The decoherence time (14) is long enough to allow all these processes to take place in the following order:

- (i) The *initial entanglement*: the system of tubulin dimers in the fundamental hexagonal unit of the (distorted) honeycomb lattice in an MT gets entangled upon the action of an external stimulus. At this stage we should remark that there is a ‘democracy’ among the fundamental hexagonal units of an MT dimer Lattice. Any unit in the lattice that gets excited by an external stimulus, behaves in the same way, getting entangled (“quantum wired”) with the rest of the units across the MT.
- (ii) The *decision-making* process : this implies the choice of the optimal path for energy and signal/or information transduction in a dissipation-loss, efficient way. To put it differently, upon the action of an external stimulus, the MT dimers system collapses, within the decoherence time (14), to one of the solitonic states mentioned in section II [7]. We stress that we view the “classical” solitons as either coherent quantum states, or minimum entropy pointer states [16], which are different from the coherent states, and are associated with incomplete collapse processes. The precise form of solitons obtained from the relevant collapse process depends on the external stimulus and environmental conditions, the kind of process/“computation” executed by the MT system, as well as the stability of the soliton. The most efficient scheme, of *maximal stability* to transport energy and information are double helices of left-right moving helicoidal sn-oidal waves, mimicking the stable structures of the DNA [47], as discussed in section II (see also footnote 3). In terms of the fundamental quDit of fig. 5(a), a double helix is formed by the initial entanglement and subsequent collapse of, say, the 2,0,6 dimers, and dimers along this direction, in such a way that a “left-moving” helicoidal sn-wave involving those is formed. The other branch of the double helix involves the 3,0,4 (and collinear dimers) along the “right-moving” helical sn-oidal wave. The double helix extends along the entire MT, while the loss-free energy- or signal transduction takes place within the time interval (14). The kinks or sn-oidal waves along the principal axis of the MT, which involve dimers in the direction of 1,0,5 in fig. 5(a), are not as mechanically stable as the double helix, and in this sense they are not as efficient as the former for the process of energy and signal/information transduction. On the other hand, the localized spike solutions may be relevant for memory switching, as discussed in [62].
- (iii) The *energy or information transfer process*: This takes place during, or even after, the collapse along the double helix soliton, which is a solution of the classical (after the collapse) pseudospin model, proposed in [7], and reviewed in section II.

If the above mechanism is realized in nature, then the tubulin dimer system of (brain) MT, or even the MT networks (see fig. 3), can operate as room temperature biological quantum biocomputers, as far as certain processes in the brain are concerned. We should stress that, given the enormous number, of order of 10^{12} , of tubulin dimers in a typical MT, this would imply an enormous computing power on behalf of the MT their networks. We stress once again that for these considerations to be valid, relatively long decoherence times of order (14) are required, which characterize the cavity QED model of MT [3, 4], as a result of the strong dipole-dipole interactions bwtween tubulin dimer dipole quanta and ordered-water dipole quanta [51]. Unfortunately, short decoherence time or order of a few hundreds of fs, as those characterizing the models of decoherence of tubulin dimers discussed in [34] or [53], although appropriate for the light harvesting antennae of Marine Algae [20, 21], where the entanglement extends over distances of order of 40 Angströms, they are not suitable for quantum computation in MT, where much longer distances of entanglement are required for efficient quantum computation.

We also stress here that our model for quantum computation involved decoherence mechanisms induced by ordinary non-gravitational environments, as expected to be the case for MTs. In this respect we differ in our conclusions from those of [15], where quantum gravity is argued to be the main source of decoherence, due to the fact that some

critical mass has been reached by the network of tubulin dimers in an MT. In our scenario of cavity QED model of MT [1, 3, 4], the electromagnetic in origin dipole-dipole interactions, are the ones that dominate over any other interaction, including the weak quantum gravitational one, and are responsible for sufficient environmental shielding of the MT so as to guarantee the relatively long quantum coherence times.

Another question is whether, via dissipation-free information and energy transmission, quantum computation could be sustained. Here is where the analogy with the "quantum wiring" encountered in marine algae, as discussed in the introduction [20, 21] serves as an appropriate perspective. There is a direct analogy of the MT system with the algae system, provided we account for the effects of ordered water, which, while traditionally underappreciated has strong enough dipole-dipole interactions [3], to provide the necessary environmental isolation so that quantum effects in tubulin dimers experience decoherence times (14), of order μs -clearly potentially relevant to many other processes taking place in a living cell as well.

V. TOWARDS EXPERIMENTAL VERIFICATION

In this section we discuss an experimental path to be followed in order to falsify the aboved theoretical (QED cavity) models of MT [1, 3, 4]. By verifying experimentally the most important features of these models, we shall also strengthen the assumption on their potential rôle in (quantum) Biocomputation.

A. Testing the Cavity-MT Model: Rabi-Splitting

One of the first tests of the QED-cavity model of MT, proposed in [3] could be the search for the well-established Rabi-splitting phenomenon [63], which is characteristic of electromagnetic cavities [6]. According to this effect, upon the action of an external (*e.g.* laser) field, of frequency Ω on *near-resonant* cavities, containing (quantum) atoms of characteristic frequency ω_0 , in interaction with the coherent photon modes inside the cavity of frequency $\omega = \omega_0 - \Delta$, with $\Delta/\omega_0 \ll 1$, the absorption spectrum of the atoms will peak at two frequencies:

$$\Omega = \omega_0 - \frac{\Delta}{2} \pm \frac{|\Delta|}{2} \left(1 + \frac{4\lambda^2 N}{\Delta^2}\right)^{1/2}, \quad (31)$$

where λ is the so-called Rabi coupling, pertaining to the atom-photon interactions, viewing the atoms as spin-1/2 two-state quantum systems, and N is the number of atoms inside the cavity. Representing each tubulin in a MT as a two-state (α , β conformations) "atom" in a cavity near the dimer walls, induced by the strong dipole-dipole interactions between the dimers and the ordered-water molecules, we covered in detail in [3] showing that a Rabi-like phenomenon similar to that in (31) could be used to characterize these entities at ambient temperatures, during the short decoherence time (14), which is itself linked to the magnitude of the Rabi coupling between the tubulin dimers and the coherent modes of the water-dipole quanta [51] which play the role of "photons" in this formulation [3].

Estimating the parameters that enter the computation of the decoherence time in the cavity model of MT is challenging as it depends on a detailed description of the ordered-water molecules. In [3] it is argued that the corresponding Rabi coupling λ is provided by the expression

$$\lambda_0 \sim \frac{d_{\text{dimer}} \cdot E_{\text{ow}}}{\hbar} \quad (32)$$

where d_{dimer} represents the matrix element of the electric dipole of a single dimer, associated with the transition from the α to the β conformations (for relevant physical parameter values see Table I), which provide the binary nature of the dimer quantum state in our framework, as discussed above. The quantity E_{ow} represents a typical root-mean-square (r.m.s.) value of the amplitude of a coherent dipole field mode in the ordered water [51]. As a crude estimate, taking into account that, in contrast to the dimers which lie in the surface of a MT, the ordered-water dipole quanta exist in the entire water-interior of the MT, we may borrow relevant formulae from quantum optics of dielectric cavities, to represent

$$E_{\text{ow}} \sim \left(\frac{2\pi \hbar \omega_c}{\varepsilon \epsilon_0 V}\right)^{1/2}, \quad (33)$$

where V is the (MT cylindrical) cavity volume, ε is the dielectric constant of the medium, taken in [3] to be that of water, at room temperatures, $\varepsilon \sim 80$ (*cf.* (28)), and ω_c is the frequency of the coherent electromagnetic mode ("photon" in quantum optics), which here is replaced by the coherent-dipole-quantum mode of the ordered water. As an estimate, in [3] we adopted the "superradiance" model of [64], in which ω_c is calculated from the energy difference,

$\Delta E_{\text{ow}}^{\text{principal}}$, between the two principal energy eigenstates of the water molecule, assuming that these are the dominant “coherent cavity electromagnetic modes” in this case:

$$\hbar\omega_c \sim \Delta E_{\text{ow}}^{\text{principal}} \sim 4 \text{ meV} \quad \Rightarrow \quad \omega_c \sim 6 \times 10^{12} \text{ Hz}. \quad (34)$$

As discussed in [3] this frequency is in the range of the upper bound of the assumed range of frequencies of quantum oscillations of the tubulin dimers viewed as two-state quantum systems (α , β conformations), before collapse, as per the original analysis of [15], and in [64]. Our study of MT as QED cavity models in [3] and here assumes this upper bound, and thus, in this case, the dominant cavity mode and the dimer system are almost in resonance, with a detuning satisfying $\Delta \equiv \omega_0 - \omega_c \ll \omega_0$, where $\omega_0 \sim 10^{12}$ Hz the dimer conformational quantum oscillations. In [3] when estimating the relevant number of dimers (“atoms”) in the cavity, we restricted ourselves to one-dimensional solitons formed along the protofilament of an MT. In the current work, we consider helicoidal solitons on the MT surface [7], and therefore we need to consider the number of dimers in the entire MT. For a typical moderately long MT, of length or order of a micron (μm), consisting of 13 protofilaments, there are

$$\mathcal{N} = \mathcal{O}(10^3), \quad (35)$$

dimers, each of about 8 nm long. For such a MT we have from (33):

$$E_{\text{ow}} \sim 1.3 \times 10^9 \left(\frac{\text{eV}}{\text{m}^3 \epsilon_0} \right)^{1/2} \sim 17.5 \times 10^4 \frac{\text{V}}{\text{m}}, \quad (36)$$

where we took into account that the vacuum permittivity is $\epsilon_0 = 55.26 e^2 \text{ eV}^{-1} (\mu\text{m})^{-1}$. On the other hand, for an MT of length 25 μm , we obtain $E_{\text{ow}} \sim 3.5 \times 10^4 \frac{\text{V}}{\text{m}}$.

Taking into account that each dimer has a mobile charge (positive or negative) $36e$, with e the positron charge, with electric dipole moment [1]: $d_{\text{dimer}} \sim 3 \times 10^{-18} \text{ Cb} \times \text{Angström}$. This implies a total the Rabi splitting for the MT

$$\lambda_{\text{MT}} = \sqrt{\mathcal{N}} \lambda_0 \sim 1.2 \times 10^{12} \text{ Hz}. \quad (37)$$

A typical detuning considered in [3] is such that $|\Delta|/\lambda_0 \sim \mathcal{O}(10^2)$, implying a situation that $\lambda_0^2 \mathcal{N} \ll |\Delta|$, which implies an approximate Rabi splitting for the case of a typical MT arrangement in the biological cells [3]:

$$\Omega \simeq \omega_0 \pm \frac{\mathcal{N} \lambda_0}{|\Delta|^2} + \mathcal{O}(\Delta). \quad (38)$$

We remark at this point that, in typical Rabi splitting situations in quantum optics it is assumed that practically no energy exchange takes place between atoms and cavity modes. In the MT case, this may be guaranteed from the fact that, since the dominant interactions between ordered-water coherent dipole models (“cavity” modes in this analogue) and dimer-dipole quanta (“atoms”) attenuate with the cubic power of the distance between them, the only dominant interactions are near the walls of the MT, thereby implying that the bulk of the cavity modes (viewing the entire MT as an isolated cavity) does not exchange significant amount of energy with the dimers. This lead us in [3] to assume that the main reason of decoherence is the leakage of dipole quanta from the MT interior to the environment, which lead to the principal estimate of decoherence time (14), which is much larger than the decoherence time (29) of [53], based on individual dimer dipole-environment interactions, outside the cavity model.

B. Probing quantum coherence and environmental entanglement of individual tubulin dimers

We assess the feasibility of experimental quantum information processing in neuronal microtubules by modeling tubulin heterodimers as multilevel quantum systems (quDits) capable of sustaining entanglement. By comparing the coupling strengths of tubulin dipoles to both evanescent surface plasmon fields and transient electric fields from neuronal action potentials, we find interaction energies within experimentally accessible regimes. These results support the use of photonic probes, such as surface plasmon resonance (SPR), for detecting coherent dipole dynamics in microtubules anchored to functionalized surfaces. Given their intrinsic dipole moment and quasi-periodic cylindrical geometry, stabilized microtubules—particularly those organized by microtubule-associated proteins (MAPs) in axonal architectures—emerge as structurally viable candidates for biologically compatible quantum information substrates [1, 3, 7]. As derived earlier, solitonic excitations such as snoidal or helicoidal waves that can propagate along MTs emerging from coherent dipole alignments [7].

A framework for quantum information processing arises when treating each tubulin dimer as a multi-level quantum system—a quDit—with its state space shaped by conformational, electrostatic, and spatial degrees of freedom. Unlike standard qubits, which encode information in binary $|0\rangle$ and $|1\rangle$ states, these quDits may operate across $D > 2$ discrete states due to the geometrical asymmetry and interaction potentials in each MT unit cell [3, 49]. This assignment is justified by the distinct roles played by the seven (including the central one, see fig. 5) heterodimers discussed previously, comprising the hexagonal MT lattice unit, which differ in angular orientation, dipole alignment, and microenvironmental exposure [7].

Dipole–dipole interactions between adjacent tubulin dimers, modeled as quantum spin operators, form the effective mechanism for quDit coupling. These interactions are short-range and scale with r^{-3} , favoring nearest-neighbor interactions and enabling controlled state entanglement within a unit cell and across adjacent MT filaments [3, 7]. The presence of ordered water molecules within the MT lumen further enhances environmental shielding and extends decoherence timescales to the microsecond regime under physiological conditions [3, 51], potentially allowing biologically useful quantum operations to occur before classical collapse.

TABLE I. Physical parameters relevant to quantum effects in biological systems. In this table we collect all physical parameter values salient to our calculations and assumptions used in prior sections throughout the present text.

Parameter	Value	Significance
Tubulin dimer dipole moment	$\sim 1.7 \times 10^3$ Debye	Strong electric fields in microtubules [73].
Microtubule diameter	25 nm	Structural scale of neuronal MT
Internal microtubule field	10^5 – 10^7 V/m	Comparable to semiconductor devices [79]
Quantum coherence time	10^{-5} – 10^{-4} s	Sufficient to underlie critical biological processes (e.g. cryptochromes in avian magnetoreception [77])
Photosynthetic coherence time	300 fs	Room-temperature quantum transport
Decoherence time - MT model of [1, 3]	10^{-6} s	quantum biocomputation

To quantify the feasibility of such operations, we estimate the strength of interaction between the tubulin dipole and external fields. Referring to tables I and II: for surface plasmons launched on nanostructured gold substrates, the evanescent field at a distance of 100–200 nm into the aqueous medium can reach magnitudes of $E_{\text{plasmon}} \sim 10^5$ V/m. Using a typical tubulin dipole moment $p \approx 1700$ D $\approx 5.67 \times 10^{-27}$ C·m [65], the resulting interaction energy is

$$\Delta E_{\text{plasmon}} = pE_{\text{plasmon}} \approx 0.35 \text{ meV}. \quad (39)$$

By contrast, during a neuronal action potential, the membrane depolarizes by approximately $\Delta V_{\text{mem}} \sim 0.1$ V. At a distance of $r \sim 500$ nm into the axon, where microtubule bundles typically reside, the induced radial electric field is

$$E_{\text{axon}} = \frac{\Delta V_{\text{mem}}}{r} \approx 2 \times 10^5 \text{ V/m}, \quad (40)$$

leading to a coupling energy of

$$\Delta E_{\text{axon}} = pE_{\text{axon}} \approx 0.71 \text{ meV}. \quad (41)$$

Both values fall within the sub-meV regime and are below thermal fluctuations at $T = 310$ K ($k_B T \approx 27$ meV), and far below the energy associated with GTP to GDP hydrolysis ($\simeq 317$ meV). Notably, the coupling energy from action potentials is approximately twice that of the lowest plasmonic interaction.

These values are 2–3 orders of magnitude smaller than $k_B T$, implying that such weak fields alone are insufficient to induce dipole state transitions in thermal equilibrium unless enhanced local fields are used such as those created by defects or nanostructures at a conducting surface. Even without such assistance (which can increase the field strength by several orders of magnitude locally), in the structured environment of the microtubule interior—particularly when interacting with ordered water and neighbouring dipoles—these couplings may contribute to the initiation or modulation of coherent quantum dynamics. In this sense, field-driven transitions may act as subtle biasing agents rather than direct triggers of quantum state evolution.

This suggests that biological activity may induce or modulate quantum transitions in MT systems via electric field-driven mechanisms [66], but only upon enhancement to bring the interaction above the competing thermal bath, while the plasmonic field provides a means to optically interrogate or stimulate such quantum states without having to use living cells (action potentials' effects can be conceivably replicated using surface-mounted MT networks addressed by fields amplified by nanostructures) [67]. An analogy of trees, branches and leaves springs to mind here: while sustained wind (hydrolysis and large energy dissipation events) may create waves in branches or even whole trunks,

TABLE II. Compiled physical, chemical, and quantum parameters relevant to the study of microtubules as potential substrates for quantum information processing. All values correspond to physiological (“ambient”) conditions we have defined as (37° C, pH 7.2, salinity ~ 150 mM), and where applicable, values are normalized or expressed in units of thermal energy (kT), GTP hydrolysis energy, or standard quantum energies. experimentally) Dielectric constant of tubulin and MTs (high-frequency): $\kappa = 8.41$. High-frequency polarizability of tubulin: $\alpha = 2.1 \times 10^{-33} \text{ C m}^2/\text{V}$. Sources include both theoretical predictions and experimental results across cryogenic and biological regimes. We also note the finding of electrical oscillations of bundles of microtubules in the brain [37].

Parameter	Value	Units	Citation / Note
Thermal energy $k_B T$ at $T = 310^\circ \text{ K}$	4.3×10^{-21} ~ 27 ~ 15.7	J meV $k_B T$ units	
GTP→GDP hydrolysis energy	~ 0.42	eV	[33]
Dipole moment of tubulin dimer (GTP state)	~ 1700	Debye	$\approx 5.7 \times 10^{-27} \text{ C}\cdot\text{m}$ [65]
Dipole moment angle change (GTP→GDP)	$\sim 27^\circ$	degrees	Conformational shift upon hydrolysis[33]
Microtubule protofilaments	13	unitless	Standard MT structure [33]
Helical pitch	~ 12	nm per turn	
Outer diameter	25	nm	[33]
Inner lumen diameter	14–15	nm	
Tubulin monomer mass	~ 50	kDa	α or β subunit[65]
Tubulin dimer mass	~ 100	kDa	Heterodimer
Typical microtubule length (neuronal)	1–100	μm	Varies with cell type[33]
Cryptochrome decoherence time	$> 10^{-5}$	s	Predicted, bird magnetoreception [77]
Photosystem I coherence time	300–800	fs	[78]
Light harvesting complex (FMO) coherence	> 300	fs	Room temp evidence [78]
Photosynthetic quantum efficiency	~ 0.95	unitless	[78]
Soliton propagation speed (microtubules)	2–20	m/s	Nonlinear excitations [33]
Time for soliton to travel 1 μm	50–500	ns	$\tau = \frac{1\mu\text{m}}{v}$
SPR evanescent field strength	10^4 – 10^5	V/m	Estimated for optical range [65]
Dipole-field coupling energy	$\sim 10^{-21}$	J	$\Delta E = -\vec{p} \cdot \vec{E}$, assuming $p \sim 10^{-27} \text{ C}\cdot\text{m}$
Surface plasmon group velocity	$\sim 10^7$	m/s	Guided modes in nanofilms
Travel time across 1 μm	~ 0.1	ps	$\tau = \frac{1\mu\text{m}}{v}$
Physiological pH (neurons)	7.2–7.4	pH	[33]
Physiological salinity	~ 150	mM NaCl	
Effective dielectric constant ϵ/ϵ_0 (MT interior)	10 – 40	unitless	Depends on hydration and polarization [65]

gusts can also be registered as “ripples” of much faster dynamics and lower energies can still be seen as “ripples” that appear and move fast on -by comparison- slower-moving and wider-amplitude waves.

The close equivalence of field strengths from these two disparate sources underscores the dual utility of MT bundles when considering substrates for the basic science as well as the specific application to scalable, ambient temperature “wet” quantum computation: they are both responsive to endogenous bioelectrical dynamics and accessible to engineered photonic quantum probes albeit with field-enhancers necessary such as the proposed surface plasmon entanglement transduction system [68, 69], where dipole transitions in tubulin could be modulated and read via optical coherence measurements.

We conclude that MT networks, with dipolar and solitonic degrees of freedom embedded in a well-defined lattice, can plausibly perform elementary quantum operations but the requirement remains for decoherence to be sufficiently delayed -as is here seen possible by structural or environmental isolation.

Previously published simulations suggest that, under physiologically plausible parameters (pH, dipole strength), tubulin may support coherence times on the order of microseconds [70]. To probe this experimentally, we have

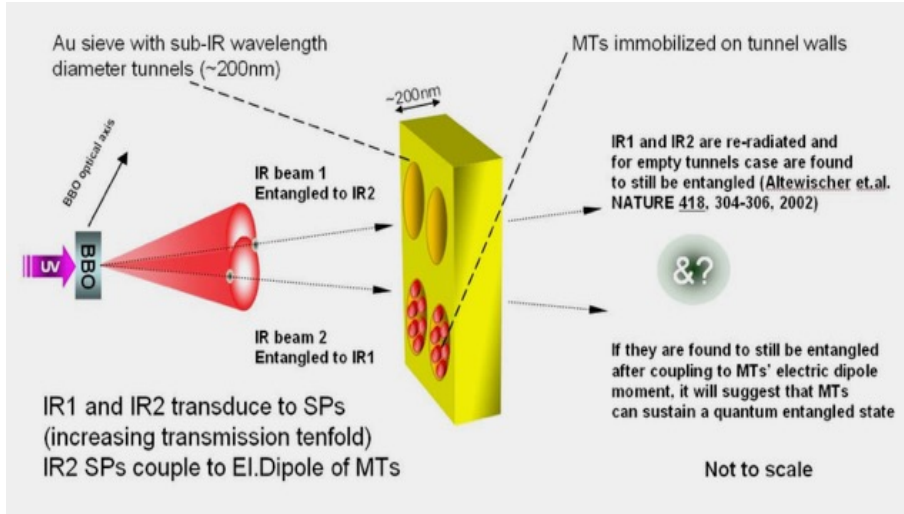


FIG. 8. A photonic entanglement transduction system, in which entangled photons are converted sequentially into surface plasmons, and then couple to protein dipole states. Representation is not to scale, and when implemented as a perforated conducting screen, it would be hundreds of tunnels per illuminated spot instead of just the four shown here. Figure taken from [68].

proposed [68] a photonic entanglement transduction system, where entangled photons are sequentially converted to surface plasmons, as has been so eloquently accomplished by Altewischer *et al.* in 2002 [69], and then couple to protein dipole states, following principles established in mesoscopic plasmonics [71] (see Figure 8).

Our case is agnostic to the details of the entangled photon pairs generation scheme, but the well-established type-II phase-matched spontaneous parametric down-conversion in a β -barium borate crystal can serve as exemplar. Such an arrangement would be producing Einstein-Podolsky-Rosen-correlated infrared photons with polarization entanglement described by the state

$$|\Psi\rangle = \frac{1}{\sqrt{2}} (|\leftrightarrow\rangle_1 |\downarrow\rangle_2 + e^{i\alpha} |\downarrow\rangle_1 |\leftrightarrow\rangle_2) \quad (42)$$

where the phase α is tunable via crystal orientation or additional birefringent elements [72].

One photon of each entangled pair is directed into a plasmonic interface based on the architecture of Altewischer *et al.* [69], wherein photon-to-plasmon conversion occurs via subwavelength apertures in a gold film Figure 2 of [68] reproduced here. To couple plasmons to biomolecules, it is possible to modify this setup by coating the perforations with a monolayer of immobilized tubulin dimers [33] that can be assembled into full MTs. The evanescent fields of the plasmons interact with the permanent dipole moments of the proteins, potentially transferring entanglement into molecular dipole degrees of freedom but this transfer has never been documented by experiment before. The pertinent Coulombic interactions are described in section IV, see (28). For typical values of the permittivity $\varepsilon \sim 80$, the analysis of [53] shows that such interactions yield the short decoherence time of (29) for a tubulin dimer. Here we see this as low-hanging fruit because following interaction, the plasmons that are reconverted to photons can be tested for residual entanglement with their twin photons using quantum state tomography and observation of partial or full entanglement would be strongly suggestive of coherent information transfer between light and the protein dipole system. There should be two qualitatively and quantitatively different peaks associated with the re-emission of entangled photons: those that only interacted with the metal surface and those that are emitted from the MTs via the metal surface. Prior experiments by our group confirmed the feasibility of tubulin immobilization and its optical response using surface plasmon resonance (SPR) and refractometry. We reported [73] concentration-dependent shifts in refractive index and dielectric constant of

$$\begin{aligned} \frac{\Delta n}{\Delta c} &= (2.0 \pm 0.5) \times 10^{-3} \text{ ml/mg}, \\ \frac{\Delta \varepsilon}{\Delta c} &= (0.5 \pm 0.1) \times 10^{-3} \text{ ml/mg}, \end{aligned} \quad (43)$$

in agreement with direct refractometric measurements [74].

Our own simulation [73] yielded dipole moments of 552 D and 1193 D for α - and β -monomers respectively, and 1740 D for the dimer, with polarizability $2.1 \times 10^{-33} \text{ C m}^2/\text{V}$, high-frequency dielectric constant $\epsilon_r = 8.41$ and refractive index $n = 2.90$ (which was also experimentally confirmed at 527 nm by label-free imaging of cytoskeleton of living mammalian cells by an independent group [75]). These values suggest strong coupling potential to plasmonic near-fields, making tubulin a viable candidate for quantum optical probing [76], and additional experimentally determined values of interest are listed in Table II.

By varying the plasmonic path length (200–800 nm), it should be possible to measure decoherence times and assess the persistence of entanglement post-interaction, thereby testing the viability of protein-based “bioqubits” in biological quantum computing contexts.

Finally before closing this subsection, we mention one more experimental path, which is not dissimilar to the aforementioned RNA memory transplant in snails [9], mentioned in footnote 1. Indeed, it is known that *Drosophila* can form stable olfactory memories of isotopically distinct molecules—such as deuterated odorants—in ways suggestive of vibrational encoding [18, 80], and that overexpression of tau microtubule-associated protein in their memory-encoding and microtubule-rich mushroom bodies disrupts normal memory formation and retrieval [17]. Such a behaviour is consistent with the QED-cavity models of MT function [1, 3] and is not predicted by conventional biological frameworks, in which MTs are seen as primarily structural and cell-mobility elements of the cytoskeleton, not typically seen as closely involved with learning and memory. We cannot help mentioning here that the robust findings of [9], according to which the RNA extracted from trained *Aplysia* can transfer memory-induced behavior to naïve individuals, points towards a further exploration of how such RNA molecules might engage with the MT network—along which they are known to travel, affecting synaptic formation [81]—as that would be one possible coupling route between biochemical and biophysical substrates of cellular memory. The alert reader should recall here that a known interaction of RNA molecules with MTs occurs in cell mitosis (see discussion in the first reference of [5]).

VI. CONCLUSIONS AND OUTLOOK

By integrating QED-based models of microtubule dynamics [1, 3, 4] with core principles of quantum information theory and using best available values for the salient physicochemical parameters, we conclude that our models predict that microtubules can function as multi-level qudit processors, contingent on the controllable preparation of coherent quantum states in tubulin dimers (methods for which are discussed elsewhere [33]).

In the current article, building upon an earlier representation [7] of classical MT tubulin dipole moments as a pseudospin non-linear σ -model, which admits various solitonic solutions, ranging from kinks and spikes to snoidal and helicoidal snoidal (double helix-like) non-linear wave solutions of dipole excitations, we have argued that these solitons can be viewed as coherent quantum states (or better pointer states) of tubulin dimer-dipole quanta (in the case of pointer states, the latter have not yet undergone complete collapse).

In this context we have identified the fundamental hexagonal unit of the honeycomb lattice representing the various tubulin heterodimer dipole arrangements in an MT (see fig. 4), with the fundamental unit of information storage, the so-called quDit, given that in our construction it is not the α , β tubulin dipole conformations that constitute the fundamental superimposed quantum states, but rather combinations of four dipole quantum states corresponding to the four corners of the parallelogram comprised of four out of the seven tubulin dimers that constitute the hexagonal fundamental cell (see fig. 5, parallelogram 0123 including the central tubulin dimer (0) and its neighboring dimers labelled (1,2,3)).

Upon the action of an external stimulus, the system of dimers in this fundamental parallelogram quantum fluctuates and is entangled (‘quantum wired’). Within the decoherence time of the tubulin dimers in the MT, the fundamental system makes a ‘decision’ on the optima path for signal and information/energy transduction/transport in an optimal, most efficient way, by means of the formation of appropriate solitonic states, which carry energy and signal in a dissipation-free manner. In this way, for instance, the double-helix snoidal waves are formed after the (incomplete) collapse of the various tubulin dimer quanta to appropriate pointer states [16], and they transport energy and signal in a dissipation-free way along the MT and even across the MT networks.

It is amusing to notice that snoidal waves, which here are used as information transporting entities in the MT network, appear also in the mathematical description of the dynamical equations of the pendulum. The latter provides a mechanical tool to keep track of the time. There are other ways of manipulating the information appropriately to tell the time, for instance either through definite sounds or by reading numbers on the table or the tower (turret) clocks. In particular, the turret clock for centuries was based on the pendulum, with its hands moving by means of an appropriate connection to hanging weights (pendulum). A similar role, as transporters of the passing of time, characterizes the snoidal solitonic waves of the dipole quanta in MT. There is a really good analogy between MT and turret clocks. The underlying mathematics (snoidal waves) are common to both systems. The snoidal waves are solutions of the pendulum equations of motion and of the equations of the MT systems, while the aforementioned

conjunction of the turret clock hands to pendulum-type hanging weights also finds a nice analogy with the MAPs connecting the various MTs in a network (*cf.* fig. 7), which as we have discussed above and in [1] can also imply the operation of MT networks as logic gates (classical or quantum).

In the present article we have discussed a QED cavity model for MT [3, 4], in which the ordered water interior of the MT operates as a highly isolated cavity, the interior walls of which are comprised by the tubulin dipole quanta. The strong interactions between the dimer dipole quanta and the dipole quanta of the ordered water near the walls imply a high-quality isolated cavity, with the main source of environmental entanglement being the leakage of water dipole quanta through the imperfect tubulin-protein-dimer walls of the MT cavity. As discussed in [3] and in the text above, this provides relatively long decoherence times of order 10^{-6} s, during which the entire MT network can be quantum wired (entangled) and energy and signal can be transported along a moderately long (of one micron long) MT.

We remark at this point that, in the absence of the cavity mechanism due to the strong ordered-water-dimer dipole-dipole interactions, the decoherence time of each tubulin dimer, as a consequence of the string dipole interaction with its neighboring dimers, would be significantly smaller, of order in the range $\mathcal{O}(1 - 100)$ fs (see (29)). Although the latter time suffices for quantum wiring of distances up to 40 Angströms, which is appropriate for entangling the entire algae antennae [20, 21], unfortunately is not sufficient for quantum wiring of the entire MT or MT networks. Distances of that size span only the basic heagonal cell of tubulin dimer lattice (see fig. 5). To entangle the entire MT (or even beyond, the MT networks) one needs the QED cavity model which enhances the decoherence times of the dipole quanta of the heterodimers, as discussed in the previous text,

With the above mechanism we have completed our description of the basic requirements for a potential biocomputation mechanism involving MT networks, at ambient temperatures, as outlined in the beginning of section IV [50]. Specifically, as has been requested by repeated criticism of other publications in the field, we here designate explicitly: (i) a precise description of the quantum states of the quDit, the basic storage of information unit, in our case having a dimension $D = 4$, in the simplest scenario (ii) a description of the mechanism through which the wavefunctions representing these states become entangled, including specification of the basis in which measurements of the quDit properties are performed in situ, and (iii) a detailed way of attaining quantum coherence over the required time scale so as to quantum-wire the MT efficiently. QuDit-gate operations in this framework are realized via dipole-dipole and dipole-field interactions, while solitonic excitations offer a plausible mechanism for coherent, low-loss quantum state transfer. This framework provides a biologically grounded platform for investigating quantum information processing in biotechnological, experimental settings, as the one proposed in Figure 7, and we propose that doing so can be used in advancing the prospect of scalable quantum computing.

For convenience we have assembled tables I and II, where typical values of parameters that are relevant to proposed quantum (computation) values in biosystems, to be compared with the pertinent parameters of our cavity model of MT reviewed here. Using MTs as the substrate for biocomputers can only be resolved experimentally by performing experiments such as those proposed here and elsewhere in the literature. Another potential path is to attempt manmade quantum computers following the example of the MT, but using appropriate spin systems to construct the basic structures.

Affaire à suivre....

ACKNOWLEDGMENTS

The work of N.E.M. is supported in part by the UK Science and Technology Facilities research Council (STFC) under the research grant ST/X000753/1. NEM also acknowledges participation in the COST Association Actions CA21136 “Addressing observational tensions in cosmology with systematics and fundamental physics (CosmoVerse)” and CA23130 “Bridging high and low energies in search of quantum gravity (BridgeQG)”. AM wishes to acknowledge the support received from www.RealNose.ai and the intellectual boost received from participants of the www.Osmocsm.Org MIT conferences and the MIT IAP class “Making Sense of Scent”.

-
- [1] N. E. Mavromatos, A. Mershin and D. V. Nanopoulos, *Int. J. Mod. Phys. B*, **16**, No. 24 3623-3642 (2002), and references therein.
- [2] See, *e.g.*: P. Dustin, *MicroTubules* (Springer, Berlin 1984); Y. Engleborghs, *Nanobiology* **1**,97 (1992).
- [3] N. E. Mavromatos and D. V. Nanopoulos *Int. J. Mod. Phys. B* **11**, 851 (1997); *ibid.* **12**, 517 (1998); *Adv. Struct. Biol.* Vol. **5** 283 (1998).
- [4] N.E. Mavromatos, *Bioelectrochemistry and Bioenergetics* **48**, 273 (1999).

- [5] D. V. Nanopoulos, [arXiv:hep-ph/9505374 [hep-ph]] (1995), invited plenary talk at the 1st International High-energy Physics Conference: The Four Seas Conference - Physics without Frontier, ENFPC 1994; N. E. Mavromatos and D. V. Nanopoulos, [arXiv:quant-ph/9512021 [quant-ph]].
- [6] S. Haroche, and D. Kleppner, *Cavity Electrodynamics*, Physics Today **42**, 24 (1989); J. M. Raimond, M. Brune and S. Haroche, Rev. Mod. Phys. **73**, 565 (2001).
- [7] A.I. Nesterov, M.F. Ramírez M.F., Berman G.P. and N.E. Mavromatos, Phys. Rev. E **93** 062412 (2016).
- [8] Loh Teng-Hern Tan, *et al.*, Progress in Drug Discovery and Biomedical Science **3** (1), Perspective Article (2020), and references therein,
- [9] A. Bédécarrats, S. Chen, K. Pearce, D. Cai and D. L. Glanzman eNeuro **5** (3) ENEURO.0038-18. (2018).
- [10] N. S. Manton and P. Sutcliffe, *Topological solitons*, Cambridge University Press, 2004, ISBN 978-0-521-04096-9, 978-0-521-83836-8, 978-0-511-20783-9 doi:10.1017/CBO9780511617034
- [11] H. Frohlich, Int. J. Quantum Chem., **2**, 641 (1968); Nature **228**, 1093 (1970); Phys. Lett. **39A**, No 2, 153 (1972); also in *Bioelectrochemistry* (F. Guttman and H. Keyzer eds., Plenum, New York 1986).
- [12] A.S. Davydov, Journal of Theoretical Biology **66** (2): 379 (1977).
- [13] W. H. Zurek, Rev. Mod. Phys. **75**, 715 (2003), and references therein.
- [14] E. Schrödinger, *What is Life* (Cambridge University Press, 1944, reprinted 1992 [ISBN 0521427088]).
- [15] S. Hameroff and R. Penrose, J. Consciousness Studies **2** (1995), 98; *ibid.* **3**, 36 (1996); Mathematics and Computers in Simulation **40**, 453 (1996); also in *Towards a science of Consciousness*, The First Tucson Discussions and Debates, eds. S. Hameroff *et al.* (MIT Press, Cambridge MA 1996); for a review, see: Physics of Life Reviews **11**, 39 (2014).
- [16] W. H. Zurek, Phys. Rev. D **24**, 1516 (1981) doi: <https://doi.org/10.1103/PhysRevD.24.1516>
- [17] A. Mershin, E. Pavlopoulos, O. Fitch, B.C. Braden, D.V. Nanopoulos and E.M.C. Skoulakis. Learning and Memory, **11** (2), 277 (2004).
- [18] M.I. Franco, L. Turin, A. Mershin, E.M.C. Skoulakis, PNAS **108** (9), 3797 (2011). and Reply to Hettlinger: Olfaction is a physical and a chemical sense in Drosophila, PNAS August 2, Vol. 108 no. 31 (2011)
- [19] N.E Mavromatos, J. Phys. Conf. Ser. **306**, 012008 (2011)
- [20] E. Collini and G. D. Scholes, Science **323**, 369 (2009).
- [21] E. Collini, C.Y. Wong, K.E. Wilk , P.M.G. Curmi, P. Brumer, and G.D. Scholes, Nature **463**, 644 (2010).
- [22] G.S. Engel, *et al*, Nature **446**, 782 (2007); H. Lee, Y.C. Cheng and G.R. Fleming, Science **316**, 1462 (2007); I.P. Mercer, *et al.*, Phys. Rev. Lett. **102**, 057402 (2009).
- [23] M. Sarovar, A. Ishizaki, G. Fleming, *et al.* Nature Phys **6**, 462–467 (2010).
- [24] S. Shim, P. Rebentrost, S. Valleau, A. Aspuru-Guzik, Biophysical Journal, Volume **102**, Issue 3, 649-660 (2012), arXiv:1104.2943 [quant-ph]
- [25] A. Mershin, K. Matsumoto, L. Kaiser, D. Yu, M. Vaughn, D. Bruce, M. Graetzel, and S. Zhang, Nature Scientific Reports, **2**, 234 (2012)
- [26] F. Levi, S. Mostarda, F. Rao and F. Mintert, Reports on Progress in Physics, Volume **78**, Number 8, 082001DOI (2015)
- [27] P.S Emani, *et al.*, Nat Methods. **18**(7), 701 (2021)
- [28] S. Pal, M. Bhattacharya, S.-S Lee, C. Chakraborty, Molecular Biotechnology **66** 163 (2024)
- [29] D.P. Srivastava, V. Sahni, P.S. Satsangi, International Journal of General Systems **45**, 41 (2016)
- [30] P. Rebentrost, T.R. Bromley, C. Weedbrook and S. Lloyd, Phys. Rev. A **98**, 042308 (2018)
- [31] P.A. Karplus, C. Faerman, Current Opinion in Structural Biology **4**, Issue 5, 770-776 (1994); S. Sahu, S. Ghosh, B. Ghosh, K. Aswani, K. Hirata, D. Fujita, A. Bandyopadhyay, Biosensors and Bioelectronics **47**, 141 (2013)
- [32] M.V. Sataric, J.A. Tuszyński and R.B. Zakula, Phys. Rev. **E48**, 589 (1993). For an updated analysis see: M.V. Sataric and J. A. Tuszyński, Journal of Biological Physics **31**, 487 (2005).
- [33] A. Mershin, H. Sanabria, J.H. Miller, D. Nawarathna, E.M.C. Skoulakis, N.E. Mavromatos, A.A. Kolomenski, H.A. Schuessler, R.F. Luduena and D.V. Nanopoulos in *The Emerging Physics of Consciousness* Springer-Verlag Berlin, Heidelberg, New York, ISBN-13-9783540238904 Chapter 4: 95-170 (2006) https://doi.org/10.1007/3-540-36723-3_4, Online ISBN978-3-540-36723-9
- [34] M. Tegmark, Phys. Rev. E **61**, 4194 (2000) [arXiv:quant-ph/9907009].
- [35] J.A. Tuszyński, J.A. Brown, E. Crawford, E.J. Carpenter, M.L.A Nip, J.M. Dixon and M.V. Sataric, Mathematical and Computer Modelling **41**, 1055 (2005).
- [36] N.A. Baker, D. Sept D., J. Simpson J., M.J. Holst and J.A. McCammon, Proc. Nat. Acad. Sci. **98**, 10037 (2001).
- [37] M.d.R. Cantero, C. Villa Etchegoyen, P.L. Perez, *et al.*, Sci Rep **8**, 11899 (2018).
- [38] M.V. Sataric, Bulletin T. CXLVI Acad. Serb. Sci. et Art. **39** 1 (2014).
- [39] J.A. Tuszyński , S. Hameroff, M.V. Sataric, B. Trpisova and M.L.A. Nip, J. Theor. Biol. **174** 1055 (1995).
- [40] M.V. Sataric and J.A. Tuszyński, J. Bio. Phys., **31**, 487 (2005).
- [41] E.E. Slyadnikov, Technical Physics. **56**, 1699 (2011).
- [42] J.A. Tuszyński, T.J.A Craddock, J. Biol. Phys. **36** 53 (2010).
- [43] J. A. Tuszyński, J.A .Brown, P. Hawrylak and P. Marcer, Phil. Trans. R. Soc. Lond. A **356** 1897 (1998).
- [44] N. E. Mavromatos, D. V. Nanopoulos, I. Samaras and K. Zioutas, Adv. Struct. Biol. Vol. **5**, 127 (1998)
- [45] M. Abramowitz M., I.A. Stegun, *Handbook of Mathematical Functions with Formulas, Graphs, and Mathematical Tables* (Dover Publications 1964)
- [46] N.D. Mermin, Rev. Mod. Phys. **51**(3), 591 (1979).
- [47] S. Brahmachari and J.F. Marko, Adv Exp Med Biol **1092**, 11 (2018).
- [48] S. Sahu, S. Ghosh S., K. Hirata., D. Fujita and A. Bandyopadhyay A. Appl. Phys. Lett., **102**, 123701 (2013).

- [49] A. Muthukrishnan and C. R. Stroud, Jr, Phys. Rev. A **62**, no.5, 052309 (2000) doi:10.1103/PhysRevA.62.052309
- [50] J.R. Reimers, L.K. McKemmish, R.H. McKenzie, A.E. Mark, and N.S. Hush, Physics of Life Reviews **11**, Issue 1, 101 (2014).
- [51] E. Del Giudice, G. Preparata and G. Vitiello, Phys. Rev. Lett. **61**, 1085 (1988); For a discussion on the rôle of non-equilibrium field theory in living matter, in a more general setting see: E. Del Giudice, S. Doglia, M. Milani and G. Vitiello, Nucl. Phys. **B251** (FS 13), 375 (1985); *ibid* **B275** (FS 17), 185 (1986).
- [52] For potential implications of quantum effects in brain functioning and the associated experimental tests, the reader may be referred to the collection of relevant articles in: *The Emerging Science of Consciousness* (J.A. Tuszynski ed., The Frontiers Collection, Springer, ©Springer-Verlag Berlin, Heidelberg 2006); ISBN 3-540-23890-5), and references therein.
- [53] Z. Xiang, C. Tang and L. Xin, Chin. Phys. B **28**, No 4, 048701 (2019).
- [54] Julsgaard B., A. Kozhekin and E. Polzik, Nature **413**, 400 (2001).
- [55] N.A. Gershenfeld and I.L. Chuang, Science **275**, issue 5298, 350 (1997).
- [56] See, for instance: Mercè Pacios Pujadó, *Carbon Nanotubes as Platforms for Biosensors with Electrochemical and Electronic Transduction* (Springer Theses, ISBN: 3642440088 (2014)), and references therein.
- [57] A.K. Geim, K.S. Novoselov, Nature Materials. **6** (3), 183–191 (2007).
- [58] R. Garreis, C. Tong, J. Terie, *et al.*, Nature Physics **20**, 428–434 (2024)
- [59] S.D. Bartlett, H. de Guise and B.C. Sanders, Phys. Rev. A **65**, 052316 (2002)
- [60] J. M. Romero and E. Montoya-González, [arXiv:2505.11487 [quant-ph]].
- [61] D.L. Koruga, Annals of the N.Y. Academy of Sciences, **466**, 953 (1986); Biosystems, **23**, 297 (1990); Nanobiology, **1**, 5 (1992).
- [62] S. Sahu, S. Ghosh, K. Hirata, D. Fujita, and A. Bandyopadhyay, Appl. Phys. Lett. **102**, 123701 (2013).
- [63] G.S. Agarwal, Phys. Rev. Lett, **53**, 1732 (1984).
- [64] M. Jibu, S. Hagan, S.R. Hameroff, K. Pribram, and K. Yasue, Biosystems **32**, 195 (1994).
- [65] J.A. Tuszynski, *Comment on Orch OR*, Physics of Life Reviews 11 (2014): 79–80.
- [66] V. Lioubimov, A. Kolomenskii, A. Mershin, D. V. Nanopoulos, H. A. Schuessler, Appl Opt. **43** (17), 3426 (2004).
- [67] J.H. Kim, J.Y. Lee, E.S. Kim, *et al.* Electric field *Photonix* **4**, 8 (2023).
- [68] A. Mershin and D.V. Nanopoulos, in Chapter 7 of *Quantum Aspects of Life* (ed. Davies, P. Imperial College Press ISBN: 978-1-84816-253-2 (2008)).
- [69] E. Altewischer, M. P. van Exter, and J. P. Woerdman, Nature **418**, 304 (2002).
- [70] T. J. A. Craddock, S. R. Hameroff, and J. A. Tuszynski, PLoS Comput. Biol. **10**, e1003456 (2014).
- [71] M. Oberparleiter, C. Kurtsiefer, and H. Weinfurter, J. Mod. Opt. **47**, 233 (2000).
- [72] P. G. Kwiat *et al.*, Phys. Rev. Lett. **75**, 4337 (1995).
- [73] A. Mershin, A. A. Kolomenski, H. A. Schuessler and D. V. Nanopoulos. Biosystems **77**, 73 (2004).
- [74] H.A. Schuessler, A. Mershin, A.A. Kolomenski and D.V. Nanopoulos. J. Modern Optics, 50 No. 15-17, 2381-2391 (2003).
- [75] P. Bon, S. Lécart, E. Fort and S. Lévêque-Fort, Biophysical Journal, Volume **106**, Issue 8, 1588 - 1595 (2014)
- [76] J. A. Tuszynski, J. A. Brown, P. Hawrylak, and P. J. Marcer, J. Comput. Theor. Nanosci. **4**, 217 (1998).
- [77] E.M. Gauger *et al.*, Phys. Rev. Lett. **106**, 040503 (2011).
- [78] G.S. Engel *et al.*, Nature **446**, 782 (2007).
- [79] J. Pokorný, Bioelectrochemistry **63** (1-2), 321 (2004)
- [80] P. Ball, Nature News, 39 (2011)] <https://doi.org/10.1038/news.2011.39>
- [81] C. E. Holt, K. C. Martin and E. M. Schuman, Nature Structural and Molecular Biology **26**, 557 (2019).